Ferroelectric properties of P(VDF-TrFE) thin films heat treated at different temperatures

By

Umme Habiba

Department of Physics

Quaid-i-Azam University

Islamabad, Pakistan
2023

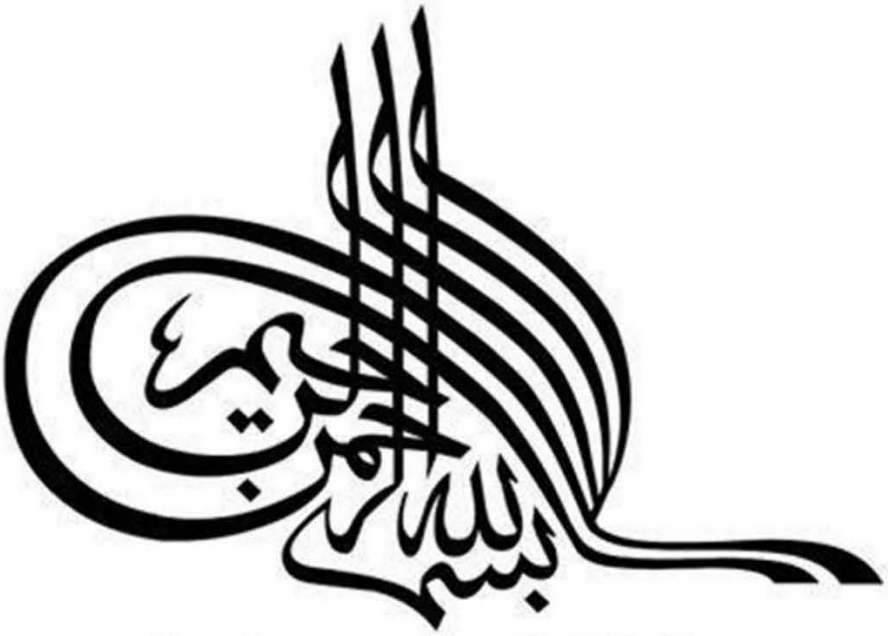

In the name of Allah,
the Most Beneficent,
the Most Merciful

This work is submitted as a dissertation

In partial fulfillment of the requirement for the degree of

MASTER OF PHILOSOPHY

IN

PHYSICS

To The

Department of Physics

Quaid-i-Azam University

Islamabad, Pakistan
2023

CERTIFICATE

This is to certify that the experimental work in this dissertation has been carried out by ***Umme Habiba*** under my supervision in the Superconductivity and Magnetism Lab, Department of Physics, Quaid-i-Azam University, Islamabad, Pakistan.

Supervisor:
Dr. Ghulam Hassnain Jaffari
Professor
Department of Physics
Quaid-i-Azam University
Islamabad, Pakistan.

Submitted Through:
Prof. Dr. Kashif Sabeeh
Chairman
Department of Physics
Quaid-i-Azam University
Islamabad, Pakistan

DEDICATION

To

My Family

Acknowledgments

I express my profound thankfulness to Allah, acknowledging that it was His divine generosity through which I was capable to overcome obstacles, gain knowledge and finish this research task. May blessings and peace be given upon last Messenger Prophet Muhammad (peace be upon him) whom many consider the ultimate example of perfection and greatness.

I am eternally grateful to Dr. Ghulam Hassnain Jaffari. His compassion, guidelines and unwavering support were critical for the timely completion of this research. I consider myself extremely fortunate for having this chance to work according to his guidance and gain from his knowledge and experience.

I am thankful to Ms. Musfira Aqeel, my senior, for offering support, direction, and useful counsel throughout the research. Her knowledge and experience have helped to shape the direction and standard of my work. I am deeply thankful to my lab mates Asra, Jihanzad, Fahad and Kainat Gul for the exchange of information and knowledge with them. In addition, I'd like to thank my friends Khadija Sattar, Khadija-tul-Kubra, Irfah Mishaal and Manahil Ashraf for their continuous support and encouragement during this journey.

I am always grateful for my beloved parents, Mr. Muhammad Saif Ullah and Mrs. Shahida Parveen, who over the years continually prioritized my education. In addition, I'd like to thank my siblings Ahmed Raza, Muhammad Fida and Umme Kulsoom for their constant support, love, care, and motivation. The unconditional love of my beloved pets Bhaloo, Tommy, Casper, Many, Cuckoo, Staphie and Ellie provide emotional support and they have all played an important role in my general well-being.

Table of Contents

Abstract xi
Chapter 1 Introduction and Background 1
1.1 Introduction: 1
1.2. Polarization: 2
1.3. Types of Polarizations: 3
1.3.1. Electronic Polarization: 3
1.3.2. Atomic or ionic Polarization: 3
1.3.3. Orientational or Dipolar polarization: 3
1.3.4. Space charge Polarization: 3
1.3.5. Spontaneous Polarization: 4
1.4. Classification of materials: 6
1.4.1. Pyro-electric materials: 6
1.4.2. Piezoelectric materials: 7
1.4.3. Ferroelectric materials: 10
1.5. Poly (vinylidene fluoride) (PVDF): 12
1.5.1. Alpha phase: 13
1.5.2. Beta phase: 13
1.5.3. Gamma phase: 13
1.5.4. Delta Phase: 14
1.6. PVDF Defects: 14
1.7. Polyvinylidene fluoride-trifluoro ethylene (P(VDF-TrFE)): 16
1.7.1. Effect of Steric hindrance on alpha phase: 18
1.7.2. Effect of Steric hindrance on Beta phase: 19
1.8. PUND Measurement: 21
1.9. Motivation: 24
Chapter 2 Characterizations and Techniques 25
2.1. Spin Coating: 25
2.1.1. Dispensing of Solution: 26
2.1.2. Spinning: 26

2.1.3. Evaporation:..... 27
2.1.4. Factors influencing film thickness:..... 27
2.2. Sonifier:..... 28
2.3. Plasma Sputter Coater:..... 29
2.4. X-ray Diffraction Technique:..... 31
2.3 Ferroelectric Measurement:..... 34
Chapter 3 Synthesis and Characterization..... 38
3.1. Thin film fabrication:..... 38
3.1.1. Substrates Cleaning:..... 39
3.1.2. Solution preparation:..... 39
3.1.3. Spin Coating:..... 40
3.1.4. Sputtering:..... 41
3.2. X ray Diffraction Pattern:..... 42
Chapter 4 Results and Discussion..... 50
4.1. PVDF-TrFE thin film ferroelectric characteristics:..... 50
4.1.1. Variation of polarization at same voltage with different annealing temperatures:..... 50
4.1.2. PUND measurement:..... 57
4.1.3. Comparative study of paraelectric component and leakage current:..... 61
4.1.4. Variation in remnant polarization at different applied signal frequency:..... 64
4.1.5. Ferroelectric Measurement using Ag-coated sample:..... 67
4.1.6. Comparison of Pt and Ag-coated samples:..... 68
4.2. Conclusion:..... 70

List of figure

Fig: 1.1 Electric dipole moment 2
Fig: 1.2 Different types of polarization [15] 5
Fig: 1.3 Classification of crystalline materials [16] 6
Fig: 1.4 Electrical signals generated by a pyro-electric material [22] 7
Fig: 1.5 Direct Piezoelectric Effect [25] 8
Fig: 1.6 Inverse piezoelectric effects [25] 9
Fig: 1.7 Hysteresis Loop displayed by ferroelectric material[30] 11
Fig: 1.8 Structures of α, β, and γ phases of PVDF [42] 14
Fig: 1.9 Steric Hindrance in PVDF Beta phase 16
Fig: 1.10 Chemical structure of copolymer [43] 17
Fig: 1.11 Effect of steric hindrance on Alpha phase [46] 19
Fig: 1.12 Effect of steric hindrance on Beta phase [46] 20
Fig: 1.13 Schematic illustration of PUND measurement [48] 21
Fig: 1.14 PUND loop indicating the polarizations measured during each pulse [48] 23
Fig: 2.1 Flow chart of experimental and characterization techniques 25
Fig: 2.2 Ossila Spin Coater [59] 28
Fig: 2.3 Branson Sonifier [62] 29
Fig: 2.4 GSL-1100X-SPC-12 Compact Plasma Sputter Coater [65] 30
Fig: 2.5 Basic illustration of Sputtering technique [66] 31
Fig: 2.6 Spectrum of X-ray radiation generated by target material [69] 32
Fig: 2.7 Principle of X-ray Diffraction [71] 33
Fig: 2.8 PANalytical Empyrean Setup 34
Fig: 2.9 PolyK Polarization Loop and Dielectric Breakdown Setup [72] 34
Fig: 2.10 Schematic illustration of Sawyer Tower circuit [74] 36
Fig: 3.1 Overview of thin film fabrication 38
Fig: 3.2 Substrate cleaning 39
Fig: 3.3 Preparation of solution 40
Fig: 3.4 Spin Coating [75] 40
Fig: 3.5 Schematic illustration of electrodes deposition 41

Fig: 3.6 XRD pattern of P (VDF-TrFE) thin films annealed at 110°C, 120°C, 130°C, 140°C, and 150°C deposited on ITO coated glass. 42
Fig: 3.7 Deconvoluted peaks for P(VDF-TrFE) films annealed at 110°C, 120°C, 130°C, 140°C, and 150°C deposited on ITO coated glass 43
Fig: 3.8 XRD patterns of P(VDF-TrFE) films fabricated from simple and distilled DMF 46
Fig: 3.9 Deconvoluted peaks for P(VDF-TrFE) films fabricated from simple and distilled DMF 47

Fig: 4.1 Ferroelectric loops of P(VDF-TrFE) thin films annealed at (a) 120°C, (b) 140°C and (c) 150°C temperatures. 52
Fig: 4.2 Current density plots of P(VDF-TrFE) thin films annealed at (a) 120°C, (b) 140°C and (c) 150°C temperatures. 53
Fig: 4.3 Hysteresis loop exhibited by films annealed at 120°C, 140°C and 150°C 54
Fig: 4.4 Hysteresis loop (a) rectangular portion (b) enlarged view of rectangular portion 55
Fig: 4.5 Trend of apparent polarization as a function of annealing temperature 56
Fig: 4.6 PUND graphs of P(VDF-TrFE) thin films annealed at (a) 120°C, (b) 140°C and (c) 150°C 58
Fig: 4.7 PUND ferroelectric loops extracted from PUND graphs 59
Fig: 4.8 True remnant polarizations vs. annealing temperature at 196V 60
Fig: 4.9 Leakage current and Paraelectric component contributions in films annealed at (a) 120°C, (b) 140°C and (c) 150°C 62
Fig: 4.10 Histogram representing Leakage current and Paraelectric component (a) LC in positive, (b) LC in negative, (c) PC in positive, (d) PC in negative directions 63
Fig: 4.11 Variation of polarization at different frequencies for thin films annealed at (a) 120°C, (b) 140°C and (c) 150°C. Arrowhead is in direction of decreasing frequency 64
Fig: 4.12 Polarization response at different frequencies (a) 120°C, (b) 140°C and (c) 150°C 65
Fig: 4.13 Ferroelectric loop of P(VDF-TrFE)/Ag thin film sample 67
Fig: 4.14 Hysteresis loops exhibited by Pt and Ag-coated samples 69

List of Tables

Table 3.1 Percentage of amorphous and crystalline regions in P(VDF-TrFE) thin films annealed at 110°C, 120°C, 130°C, 140°C and 150°C 44
Table 3.2 Percentage of amorphous and crystalline regions in P(VDF-TrFE) thin films fabricated from simple and distilled DMF 48

Abstract

Current research focuses on the ferroelectric attributes of the polyvinylidene fluoride-Trifluoroethylene (P(VDF-TrFE)) thin films fabricated through spin coating technique. After spin coating films were annealed at 110°C,120°C,130°C,140°C and 150°C. The X-ray diffraction technique was used to confirm the existence of β-phase. The degree of crystallization in the specimens was subsequently shown to vary because of annealing temperature of films. The ferroelectric characteristics of specimens were thoroughly examined. Ferroelectric loops have been obtained by subjecting the specimens to sinusoidal voltage signal. P(VDF-TrFE) films exhibited well-defined hysteresis loops, revealing the presence of switching polarization. The *positive up negative down* (PUND) methodology was used to analyze switching as well as non-switching behaviors. The true value of polarization has been extracted from the PUND measurement. The retrieved PUND loops enable us to investigate the responses of actual polarization that related to ferroelectric domain switching. A thorough comparison of apparent polarization and true polarization in samples of varying annealing temperature was performed, allowing for an in-depth understanding of the connection between them. The switching polarization and space charge polarization affects the observed value of remnant polarization at lower frequencies, leading to a greater overall value. The effect of the frequency of the applied signal is also examined on ferroelectric thin films specimens. Furthermore, the capacitor like geometry fabricated with different metal electrodes is analyzed to understand the interfacial effect.

Chapter 1 Introduction and Background

1.1 Introduction:

In the past few decades, there seems to be an evolution in technology working on ever smaller scales. This offers various advantages, including the capacity to develop materials with unique features and to use less physical space. When it pertains to work on small areas, thin films are a very attractive field for research. One of the three dimensions of a thin film is substantially smaller than the other two, leading to a high proportion of surface to volume. This means that the material's surface effects are significantly more noticeable when compared to a bulk substance [1]. Thin films possess numerous potential uses in electronic devices, optical technology, the agricultural sector, photovoltaic cells, ornamental coatings, and hard coatings [2]. A range of processes, including physical vapor deposition (PVD), sputtering, chemical vapor deposition (CVD) [3], and spin coating [4], can be employed to fabricate thin films. Researchers can use these techniques to deposit extremely thin layers of substance onto a substrate that can be modified to fulfill specific demands.

Polymers are a distinct class of materials comprised up of monomers that influence their properties. They have a chain-like structure and can be crystalline, amorphous, or a combination of the two. Polymers are softer and more malleable than ordered inorganic materials because they have weak bonding, and a disordered structure [5]. They often exhibit structural conformations. Polymers structural composition, despite their disorder, provides an effective toughness, adaptability, flexibility, compact size, and durability [6]. Polymers' biocompatibility is one of their main advantages [7], making them appropriate for use in medical applications. They also have excellent mechanical properties, are simple to process, and are inexpensive [8].

Polymer thin films have sparked great interest in a variety of technological disciplines due to their enticing properties. Because of their unique features, these materials have found applications in electronic goods, sensors [9] and actuators [10]. This chapter provides a thorough overview of polarization and its different forms, pyroelectric, piezoelectric, and ferroelectric materials. The chapter also discusses two materials that are currently under study: PVDF and P(VDF-TrFE).

1.2. Polarization:

There lie a positive charge center and a negative charge center in a molecule. Unpolarized molecules are those that have both positive as well as negative charge centers at the same position. Applying an electric field will cause a molecule's overall positive and negative charges to move. Positive charges displace in the direction of the electric field, whereas negative charges move in the opposite direction. After applying electric field unpolarized molecules become polarized and a dipole is created. So, the process of producing a dipole or dipole moment is called polarization. Dipole moments are directed from a negative charge towards a positive charge of magnitude ***q*** as shown in figure 1.1. The term "dipole moment" corresponds to the vector quantity ***p.*** When an external electric field is applied to dielectric materials, the dipole moments have a tendency to rearrange themselves through a distance ***r*** [11]. The following discussion will concentrate on the five major categories of polarization mechanisms: electronic, atomic, or ionic, orientational, space charge and spontaneous polarization.

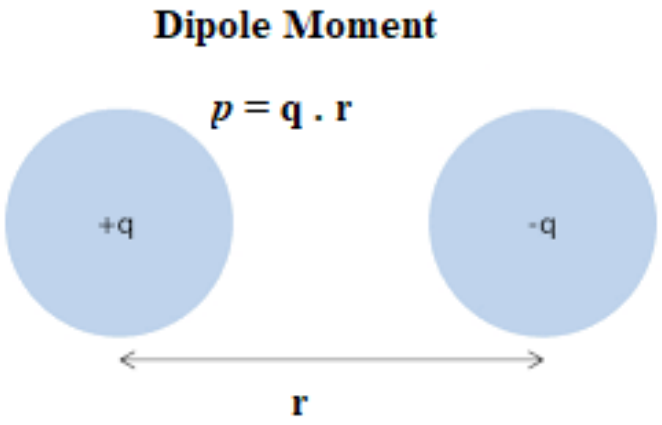

Fig: 1.1 Electric dipole moment

1.3. Types of Polarizations:

1.3.1. Electronic Polarization:

When an external electric field is not present, the center of the positively charged nucleus and the negatively charged electronic cloud is the same. However, when an external electric field is applied, the electronic cloud moves slightly from its initial position, causing one end of the atom to become positively charged and the other end to become negatively charged. This process, which is induced by the external electric field, is referred to as electronic polarization. Electronic polarization is most evident at high frequencies of alternating electric field [12].

1.3.2. Atomic or ionic Polarization:

Atomic polarization is another type of induced mechanism that takes place in molecules containing different types of atoms that share their valence electrons with each other. When an external electric field is applied, the ions in these molecules move from their original position, resulting in the creation of a dipole moment. This type of polarization is also referred to as vibrational polarization since it can disturb the normal lattice vibrations. Atomic polarization is more prominent at slightly lower frequencies compared to electronic polarization [13].

1.3.3. Orientational or Dipolar polarization:

Dipolar polarization occurs in materials that have a permanent dipole moment and an asymmetrical bonding structure that allows a net permanent dipole moment. When an external electric field is applied, the dipole moments in the material align themselves in the direction of the electric field. The degree of polarization in these materials varies depending on the direction of the external electric field [14].

1.3.4. Space charge Polarization:

When a material containing mobile charged particles is subjected to an external electric field, the charged particles flow and gather at boundaries between regions of different charges. The resultant accumulation produces a space charge layer that opposes the external electric field and causes the formation of a dipole moment. This kind of polarization is known as space charge

polarization [14] and it is observed in dielectric materials. Space charge polarization may take place in the following ways:

1) Interfacial polarization: This occurs at the interface of two materials having different dielectric constants. Charged particles collect at the contact, resulting in the formation of a space charge layer and dipole moment [14].

2) Hopping polarization: This occurs inside a homogenous material due to the existence of impurities, defects, or abnormalities in its structure. Charged particles move towards regions of lower or higher electric potential, leading in to the growth of space charge layers and the creation of a dipole moment [14].

1.3.5. Spontaneous Polarization:

Certain materials exhibit a natural polarization known as spontaneous polarization even in the absence of an external electric field. This polarization results from the centrosymmetric arrangement of atoms or molecules in the material. Spontaneous polarization arises in a specimen because there exist dipole-dipole interactions, therefore, these dipoles remain aligned in a certain direction even if the applied electric field is zero. Pyro, Piezo and Ferroelectric materials are examples of materials that display spontaneous polarization [14]. Figure 1.2 shows different types of polarization.

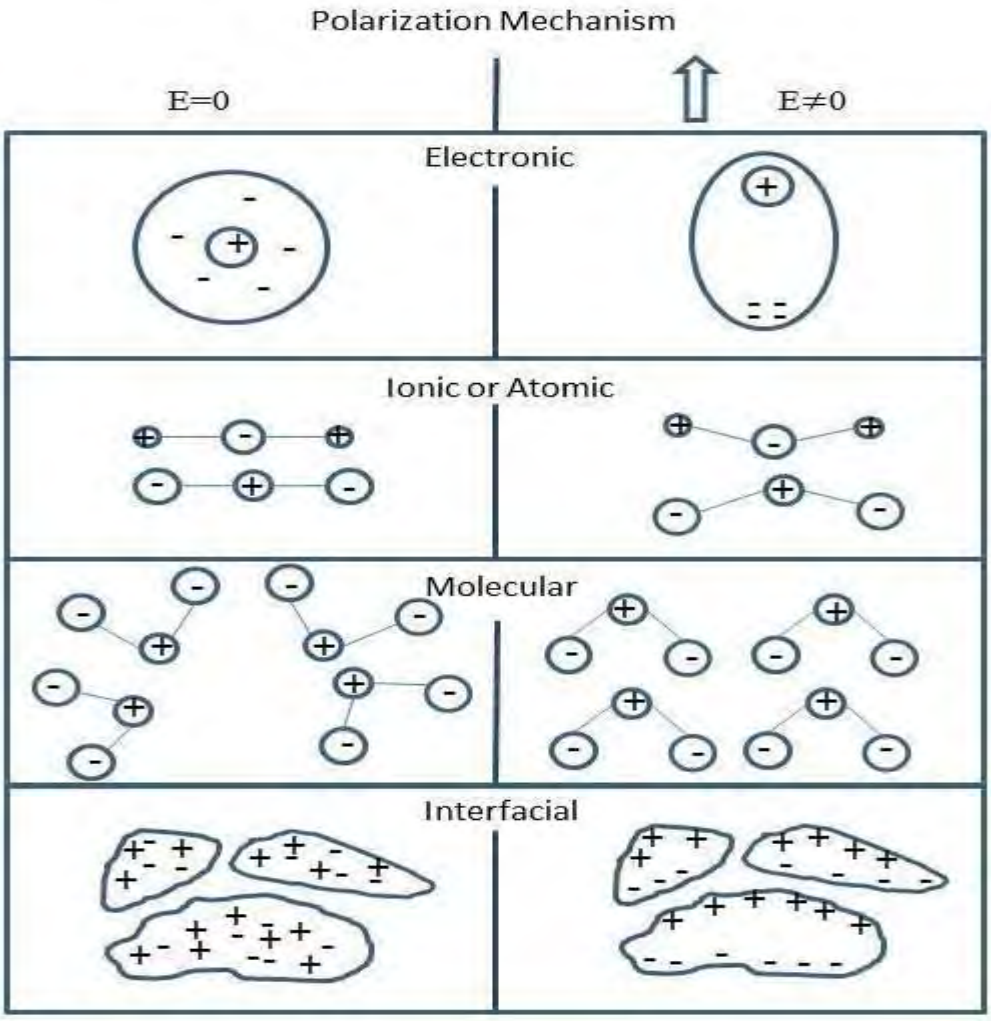

Fig: 1.2 Different types of polarization [15]

1.4. Classification of materials:

The structure of crystals is classified in 32 categories according to symmetry operations. A more comprehensive classification can be seen in Figure 1.3. The particular emphasis of this classification is on Pyroelectric, Piezoelectric, and Ferroelectric substances, those will be addressed in detail below.

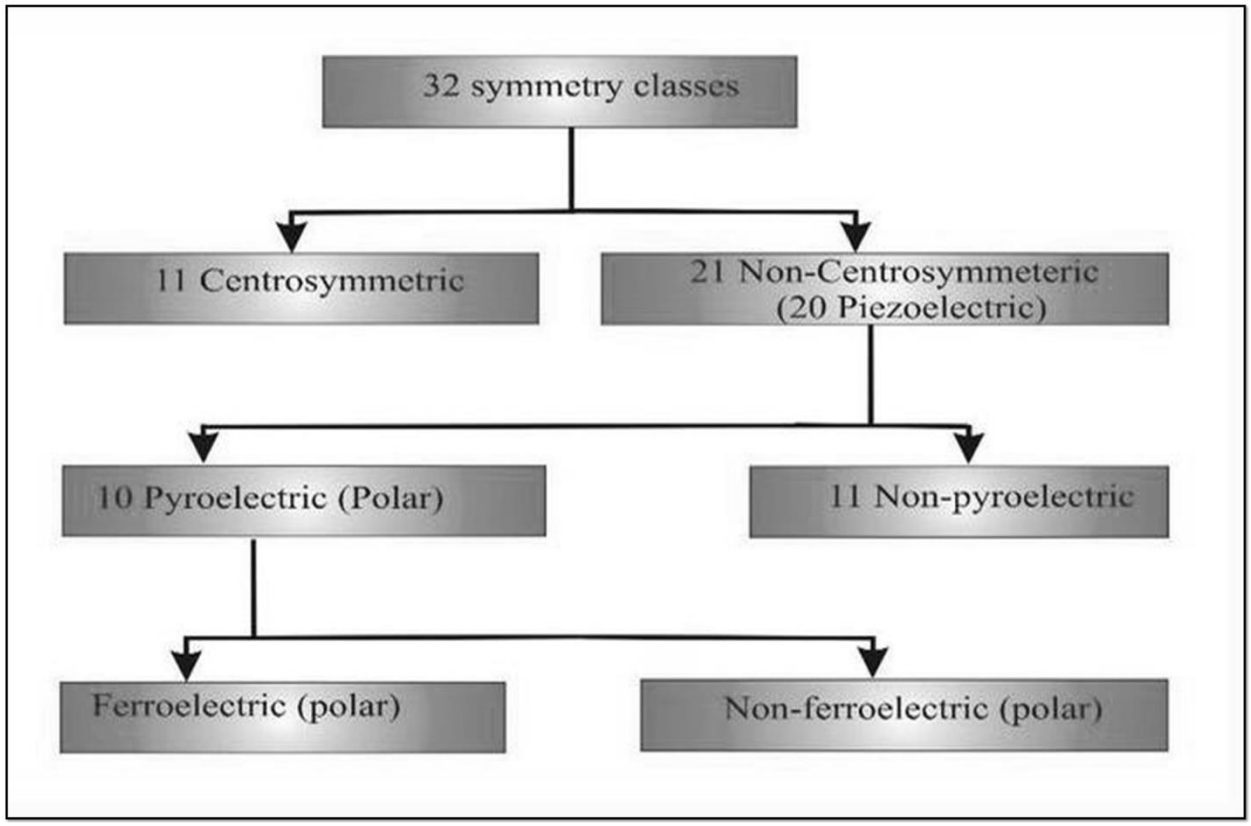

Fig: 1.3 Classification of crystalline materials [16]

1.4.1. Pyro-electric materials:

Pyro-electric materials are materials that can generate an electrical charge when exposed to temperature fluctuations [17]. The term "pyro-electric" comes from the Greek terms "pyro," which means "fire," and "electric," which means "electricity." These materials are often made up of crystals with a non-centrosymmetric crystal structure, which lacks a center of symmetry [18]. When heated or cooled, the non-centrosymmetric structure causes a movement of electrical charge within the crystal, creating an electric field and an electrical potential differential across the material. The polarity and magnitude of voltage created by Pyroelectric material are

determined by the direction and magnitude of the temperature change. The sensitivity of temperature changes of a pyro-electric material is determined by coefficient of pyro-electricity that determines the degree to which its polarization varies in reaction to temperature [19]. Because of their unique features, pyro-electric materials are frequently used in several kinds of applications, including infrared detectors [19], thermal imaging photographic equipment, sensors for temperature [20], and healthcare devices [21]. This effect is illustrated in fig 1.4 which shows temperature variation and corresponding electrical signal.

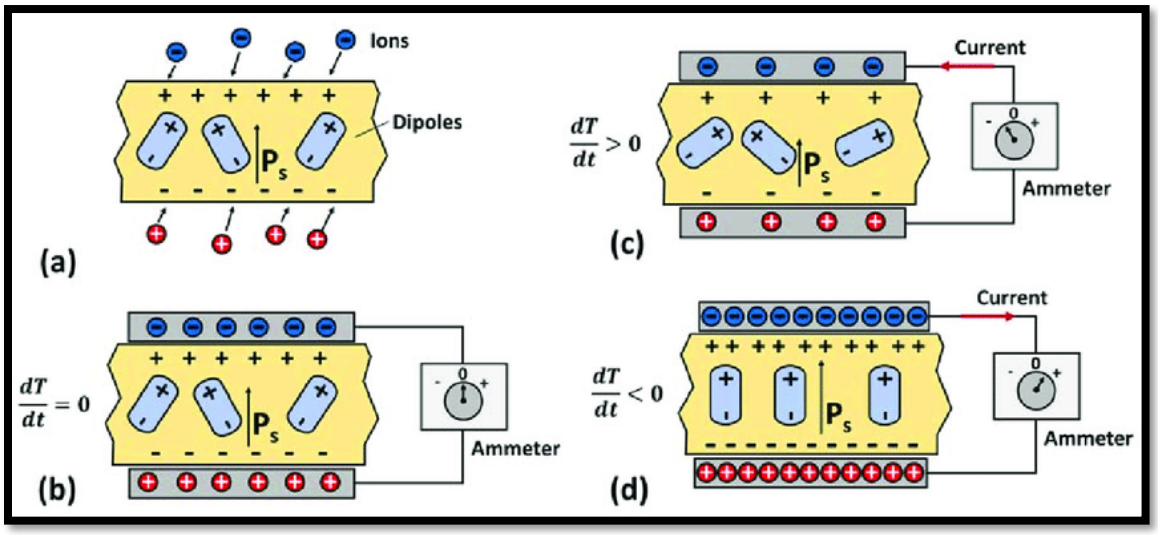

Fig: 1.4 Electrical signals generated by a pyro-electric material [22]

1.4.2. Piezoelectric materials:

Piezoelectric materials are a type of material that, due to the piezoelectric effect, may convert mechanical stress or pressure into electrical voltage and vice versa. This phenomenon is observed in crystalline materials such as quartz and ceramics. When we apply mechanical stress or pressure to a piezoelectric material, it results in an electric charge separation within the material. This separation of electric charges produces an electrical voltage across the material, which can be used to power electronic gadgets or evaluate applied force [23]. Piezoelectric materials are functional materials for sensors, actuators, and biological applications [24]. The piezoelectric effect has following two types:

a) Direct Piezoelectric effect: When a piezoelectric material is subjected to mechanical pressure or stress, an electrical voltage is generated across the material, resulting in the direct

piezoelectric effect [23]. That is, the material converts mechanical energy into electrical energy as shown in fig 1.5.

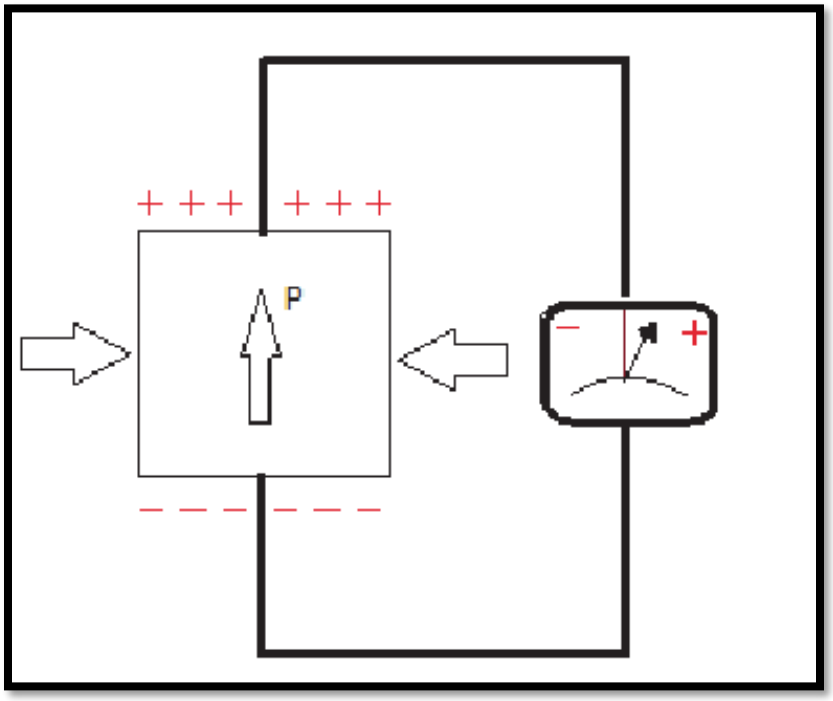

Fig: 1.5 Direct Piezoelectric Effect [25]

b) Inverse piezoelectric effect: When an electrical voltage is applied to a piezoelectric material, it deforms or changes shape due to the inverse piezoelectric effect [23]. The substance in this scenario transforms electrical energy into mechanical energy as shown in fig1.6.

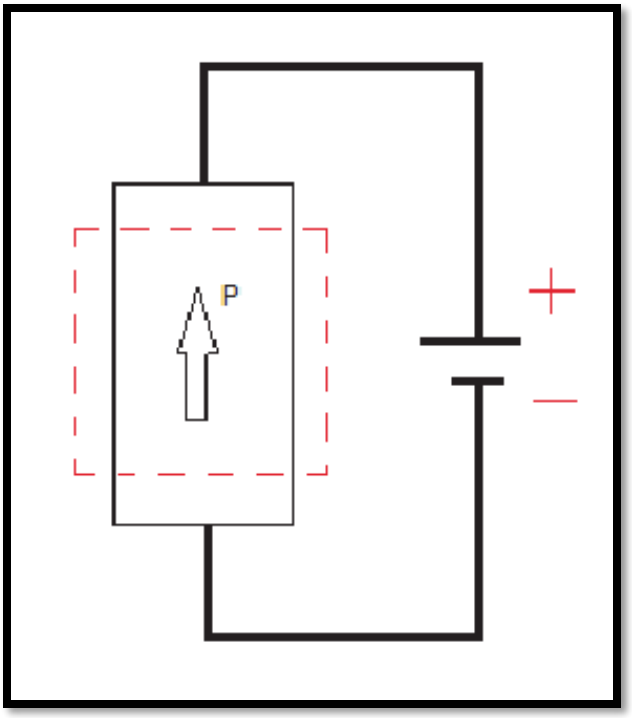

Fig: 1.6 Inverse piezoelectric effects [25]

1.4.3. Ferroelectric materials:

Ferroelectric materials have a unique crystal structure that allows for the formation of a permanent electric dipole moment and possess spontaneous polarization. An external electric field can be used to reverse this polarization. Ferroelectric substances are composed of dipoles oriented in a specific direction. But due to some factors like material's crystal structure, those dipoles usually develop into regions of different polarization directions known as domains. Each domain is a portion of material with homogeneous dipole orientation. Domain walls are places where the orientation of the dipoles progressively shifts from one domain to another at the boundaries among domains [26]. The domains electric polarization is oriented differently relative to one another. Whenever an electric field from the outside is applied, domain walls may shift, realigning the domains and inducing net electric polarization in the substance. This is known as ferroelectric switching, and it is the basis for many practical applications of ferroelectric materials. Curie temperature is the temperature at which phase transition takes place in materials that are ferroelectric. These materials have a non-centrosymmetric structure below and at Curie temperature. They have a centrosymmetric structure above Curie's temperature and possess no spontaneous polarization. Ferroelectrics are basically piezo electrics and pyro electric, whereas the opposite may not be true. Reversible spontaneous polarization is a further characteristic of ferroelectric materials [27].

1.4.3.1. Ferroelectric Hysteresis Loop:

Ferroelectric materials display a hysteresis loop below their Curie temperature, which is illustrated in figure 1.7. When a ferroelectric material is subjected to an electric field in the positive direction, the material's domains begin to align themselves in the direction of the field until the saturation polarization is reached [27]. At this point, the crystal has a single domain that is aligned with the direction of the electric field. When the electric field is removed, the polarization of the ferroelectric material decreases to a non-zero value known as remnant polarization (P_r), indicating that specific regions of its domains are still aligned in the positive direction. The direction of the electric field is subsequently reversed. As the magnitude of the negative electric field is increased, the remnant polarization eventually becomes zero at a specified value of the electric field in the negative direction, defined as the coercive field (E_C)

[28].When the magnitude of the electric field is increased in the negative direction, saturation polarization arises, which suggests all of the domains have aligned in the direction of an externally applied field. When the field is reduced to zero, polarization achieves remnant polarization in the opposite direction [29].

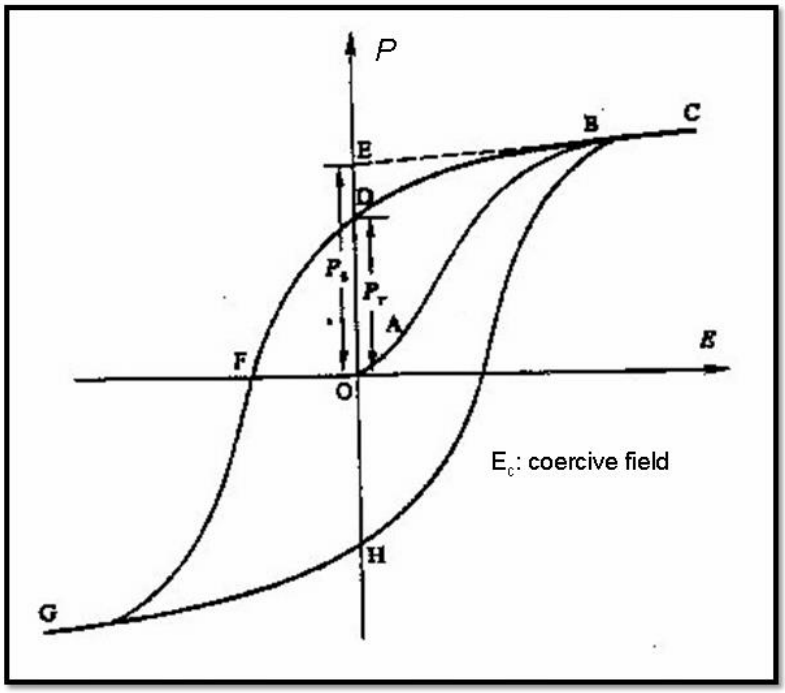

Fig: 1.7 Hysteresis Loop displayed by ferroelectric material[30]

1.4.3.2 Factors that affect loop:

The ferroelectric hysteresis loop describes the relation among applied electric field and resulting polarization. Several factors influence hysteresis loop, including:

1) Structure of Crystals: The structure of the crystals of a ferroelectric material has a major influence on hysteresis loop. The loop's shape and magnitude are determined by the crystal structure's symmetry and alignment of crystal axes.

2) Electric Field: The shape and width of hysteresis loop are affected by the magnitude of electric field that's applied to ferroelectric specimen. A stronger electric field produces more polarization.

3) Frequency: Due to impact of polarization relaxation processes, the frequency of electric field can vary the width and shape of loop.

4) Temperature: At a specific temperature known as the Curie temperature, ferroelectric materials undergo a phase transformation from ferroelectric to paraelectric. Ferroelectric hysteresis loop shifts with temperature and eventually disappears above this temperature [29].

5) Film's thickness: The ferroelectric film's thickness can alter hysteresis loop by modifying the energy needed for switching the polarization.

6) Defects: Defects and Impurities in ferroelectric substance may trigger domain wall pinning and change the shape of loop [29].

1.5. Poly (vinylidene fluoride) (PVDF):

PVDF, a material with semi-crystalline structure, has been attracting the attention of researchers due to its good piezoelectric and ferroelectric properties. Furthermore, its outstanding properties like mechanical strength, thermal and chemical stability, and high pyro and piezo coefficients make it an appealing material for a variety of applications, including sensors, detection devices, storage systems, and healthcare. PVDF, or Polyvinylidene fluoride, is a polymer comprised of - (CH_2-CF_2) - repeating units. Since the interactions between fluorine and carbon atoms are extremely strong, PVDF is highly resistant to heat and chemicals. This feature, combined with its high dielectric strength, makes it a preferred choice for adhesives, coatings, and insulating substances in a variety of industrial applications [31].

The curie temperature of PVDF is around 100 degrees Celsius, which refers to the temperature where its ferroelectric characteristics vanish. This characteristic is useful in scenarios wherein PVDF is employed as a piezoelectric substance since it enables precise regulation of material's properties [32]. PVDF has a glass transition temperature of -35°C. This temperature is significant because it marks the point at which the polymer changes from a hard, glassy state to a more rubbery, flexible state. This feature is significant in applications requiring flexibility, such as membranes and films. PVDF can exist in four major structural forms: alpha (α), beta (β), gamma (γ), and delta (δ). PVDF's ferroelectric and piezoelectric characteristics are highly influenced by its structural shape. The beta phase of PVDF, for example, is the most often utilized form in piezoelectric applications, but the alpha phase is frequently employed in coatings and membrane [31].

1.5.1. Alpha phase:

At room temperature, alpha phase of Polyvinylidene fluoride (PVDF) is the most stable, prevalent and kinetically preferred structural form [31]. The PVDF polymer chains are packed in hexagonal orientation during this phase, leading to an extremely high level of symmetry and order. Since alpha phase is non-polar in nature, the dipole moments of each of the chains of polymers have random orientations and cancel one another [33]. It has a monoclinic structure with TGTG-configuration chains [34]. Slow cooling of annealed films can result in the alpha phase, which has lattice parameters of a = 4.96Å, b = 9.64Å, and c = 4.62Å [31]. The density of this phase is around 1.78 g/cm^3 and a melting point of approximately 171 °C. Stretching can cause the alpha phase conversion to beta phase [35], whilst thermal treatments can cause conversion to gamma phase. Poling at high fields can induce the Delta phase [36].

1.5.2. Beta phase:

The beta phase is a polar, crystalline structure formed by employing external forces such as stretching by force or electric fields. In comparison to alpha phase, beta phase of PVDF possesses more organized as well as compacted polymer chains, resulting in a polar framework with a greater dipole moment [37]. The density of beta phase is roughly 1.76g/cm^3. The melting point of beta phase is around 175°C, somewhat higher compared to the melting point of alpha phase [38].

In this phase chains are organized in a TTTT pattern. The dipoles in this arrangement are perpendicular to the chain axis, and each unit cell has two chains with dipoles pointing in the same direction. In this phase, the H and F atoms are on opposite sides of the backbone chain, resulting in a non-zero dipole moment. When compared to the other phases, the Beta phase possesses superior piezo and Ferro characteristics. It has a hexagonal crystal structure with a = 8.58Å, b = 4.91Å, and c = 2.56Å lattice parameters [39].

1.5.3. Gamma phase:

The gamma phase of Polyvinylidene fluoride (PVDF) is an amorphous and non-crystalline phase which can be produced by heating the substance above its melting temperature then rapidly cooling it. The chains of polymers of PVDF in this phase are haphazardly aligned thus lack long-range order. The gamma phase separates itself from the alpha and beta phases by its distinct characteristics caused by the absence of long-range order. The gamma phase has a

higher glass transition temperature, making it more resistant to heat than alpha and beta phases [40]. Furthermore, the gamma phase has a lower dielectric constant than the alpha and beta phases, It shows T_3GT_3G' conformation and has lattice parameters of a = 8.66Å, b = 4.93Å, and c = 2.58Å [39].

1.5.4. Delta Phase:

Polyvinylidene fluoride (PVDF) delta phase is a ferroelectric phase which may be produced by introducing an electric field to the substance when it is in beta phase. When an electric field is applied, the polarized domains align in the direction of field. The material demonstrates spontaneous polarization in the delta phase, which is the polarization that exists even in absence of an electric field being applied [37].

Figure 1.8 depicts different structural configurations of PVDF [41].

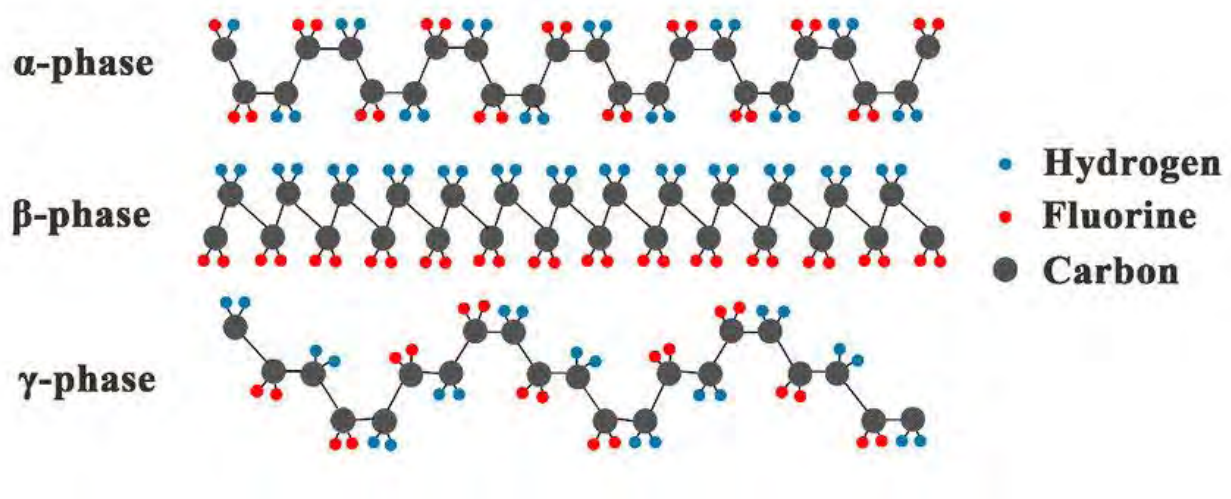

Fig: 1.8 Structures of α, β, and γ phases of PVDF [42]

1.6. PVDF Defects:

Polyvinylidene fluoride is a kind of polymer with good ferroelectric properties, making it useful in a wide range of applications including capacitors, actuators, and sensors. But the presence of defects in polymer chains may hamper PVDF performance. Due to reversal of certain monomers during the production process, PVDF may have defects in the structure of its molecules. Head-to-Head (HH) and Tail-to-Tail (TT) defects are the two types of defects that can arise. The creation of a bond between two nearby carbon atoms, each of which is likewise bound to two fluorine atoms, is involved in HH defects. In the polymer chain, this occurs in a -

($\mathbf{CF_2}$-$\mathbf{CF_2}$) - sequence. The development of a bond between two nearby carbon atoms, each of which is likewise bound to two hydrogen atoms, is involved in TT defects. In the polymer chain, this occurs in a - (C$\mathbf{H_2}$-C$\mathbf{H_2}$) - sequence. Both types of defects may arise in pairs, which are referred to as HHTT defects. The HHTT defect is distinguished by alignment of adjacent chains of PVDF polymers in a head-to-head and tail-to-tail configuration that is contrary to the polymer's conventional head-to-tail structure [37]. Since the dipole moment of the polymer is reduced by this alignment, the total polarization of the substance may be reduced because of this disruption. It causes a kink within the chains of polymer, making it less aligned and less capable of maintaining a polar structure. Thus, these defects influence the physical and mechanical aspects. HHTT defects cause steric hindrance among F atoms in neighboring chains increasing the system's energy. The energy of Alpha phase increases due to steric hindrance and causes the system to achieve a new stable state and, therefore, phase conversion may occur. Defect density less than 10% favors the Alpha phase formation. On the other hand, beta phase can endure HHTT defects more than alpha phase as shown in fig 1.9.Defect density more than 12% cause the Beta Phase configuration to be favorable, resulting in the presence of Ferro electricity inside PVDF [41].

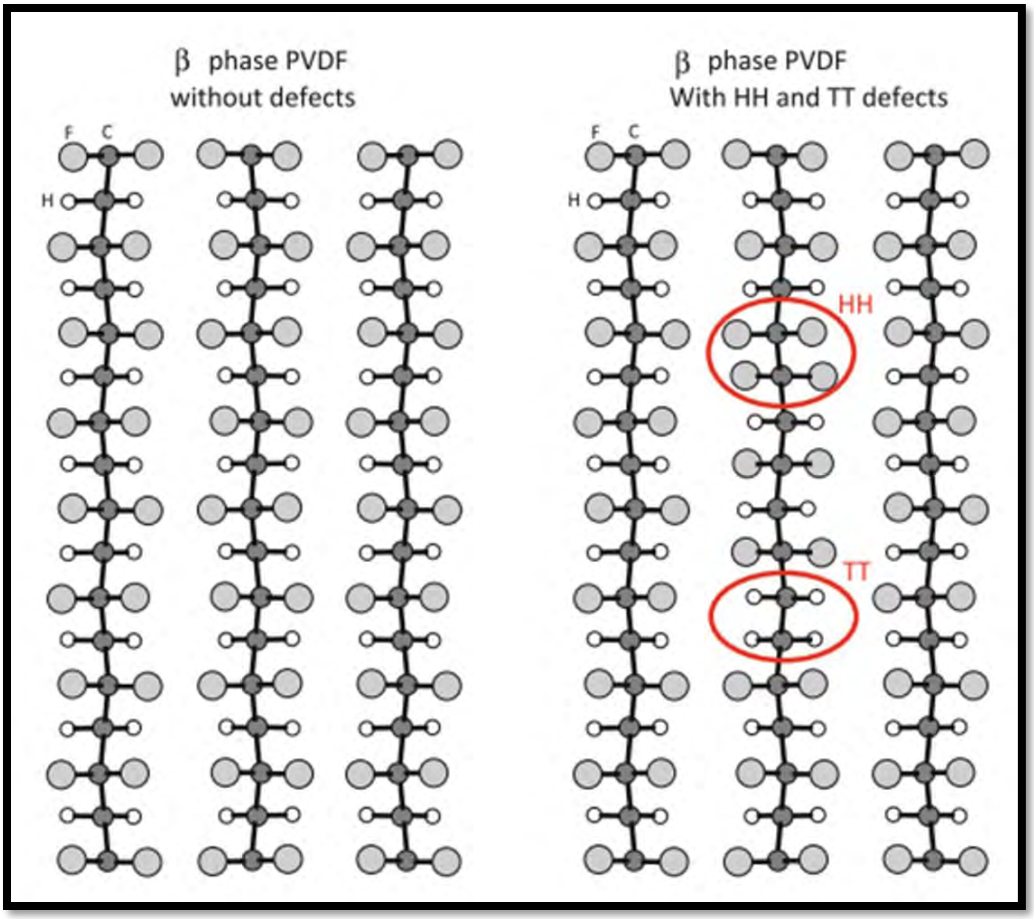

Fig: 1.9 Steric Hindrance in PVDF Beta phase

1.7. Polyvinylidene fluoride-trifluoro ethylene (P(VDF-TrFE)):

Polyvinylidene fluoride-trifluoro ethylene (P(VDF-TrFE)) is a copolymer formed by mixing the monomers PVDF and PTrFE. The chemical formula for copolymer is shown in fig 1.10

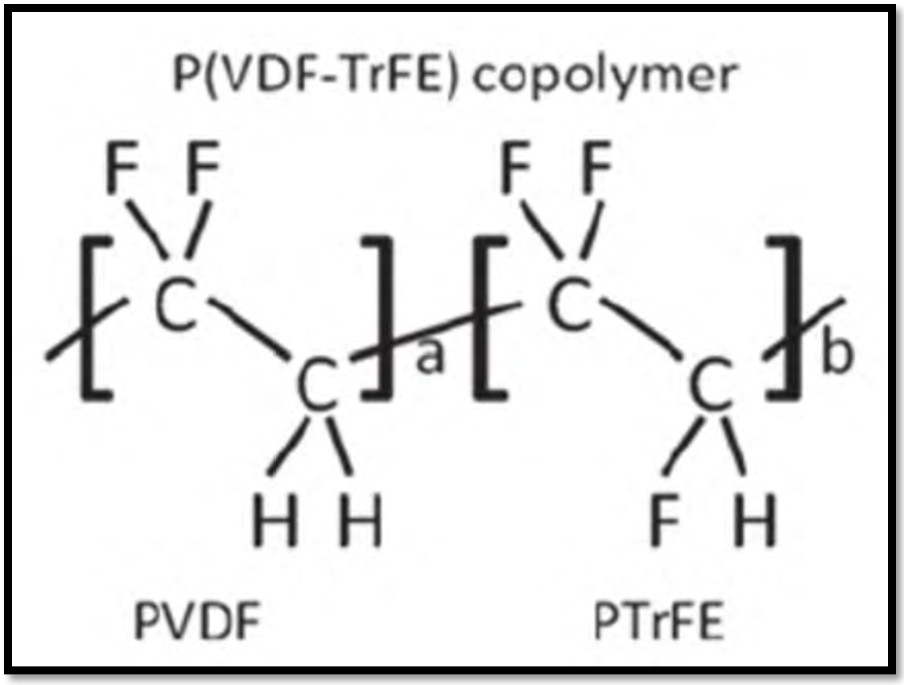

Fig: 1.10 Chemical structure of copolymer [43]

The resulting copolymer has a distinct blend of features derived from both monomers, making it a versatile material in a wide range of applications. It possesses a semi-crystalline configuration, which indicates that its molecular arrangement has both ordered and disordered areas. P(VDF-TrFE) has comparable structural group to PVDF at lower temperatures that is orthorhombic with just a minor increase in lattice parameters [44]. But, at higher temperatures, the copolymer has a hexagonal structure .Furthermore, at a molar percentage of 20-35%, it can transform into Beta phase without any post-treatment [45]. This transformation can increase the crystallinity of copolymer up to 90%. PVDF and its copolymers incorporating TrFE display piezoelectric efficiency and high remnant polarization. The optimal TrFE content range for achieving ferroelectric characteristics is between 90/10 – 70/30. However, exceeding this range of TrFE content can result in deterioration in the ferroelectric characteristics of material, possibly due to a reduction in the size of the crystallites [41]. The incorporation of TrFE monomers in PVDF to produce the copolymer P(VDF-TrFE) causes steric hindrance. This hindrance is mostly caused by bulky fluorine atoms found in TrFE monomers that can disturb the copolymer's molecular packing and chain orientation. The degree of steric hindrance varies with the amount of TrFE in copolymer, with larger TrFE contents resulting in greater degree of hindrance. This steric hindrance can affect the crystallinity, ferroelectric characteristic, and piezoelectric

efficiency of the copolymer [46]. Thus, due to the steric hindrance, caused by the TrFE monomers the alpha phase of PVDF can be converted into desirable ferroelectric Beta phase by adding an optimum amount of TrFE monomers.

1.7.1. Effect of Steric hindrance on alpha phase:

Steric hindrance is the phenomena of repulsion between atoms or groups of atoms caused by differences in size, shape, or arrangement. The steric hindrance established by the TrFE monomers in the alpha phase of P(VDF-TrFE) can have significant effects on the copolymer. This phase has a highly ordered and crystalline molecular structure; however, the addition of TrFE monomers can disrupt this arrangement and result in a less ordered structure, lowering the crystallinity and ferroelectric characteristics of the copolymer. Furthermore, the steric hindrance formed by TrFE can reduce the piezoelectric efficiency of the copolymer. The degree of steric hindrance, on the other hand, can be regulated by varying the quantity of TrFE in the copolymer. Lower TrFE concentrations can reduce the hindrance whereas larger amounts can have a greater impact [46]. Effect of steric hindrance on Alpha phase is shown in fig 1.11.

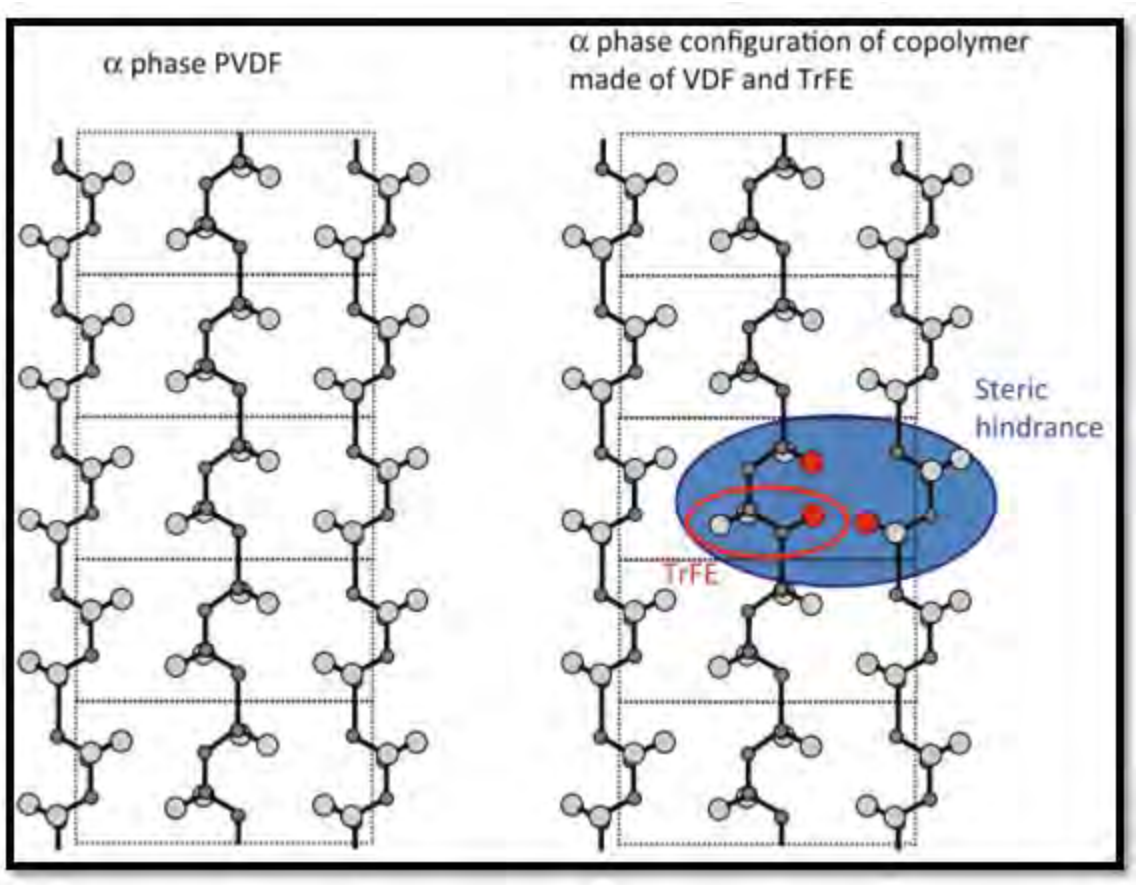

Fig: 1.11 Effect of steric hindrance on Alpha phase [46]

1.7.2. Effect of Steric hindrance on Beta phase:

PVDF's beta phase consists of a highly structured and closely packed crystal structure, which accounts for the material's polar characteristics. TrFE monomers feature a bulky side group that may create steric hindrance during crystallization, that alter crystal structure and characteristics of PVDF beta phase. The steric hindrance imposed by TrFE monomers has no influence on the beta phase of PVDF [46], as illustrated in fig 1.12.

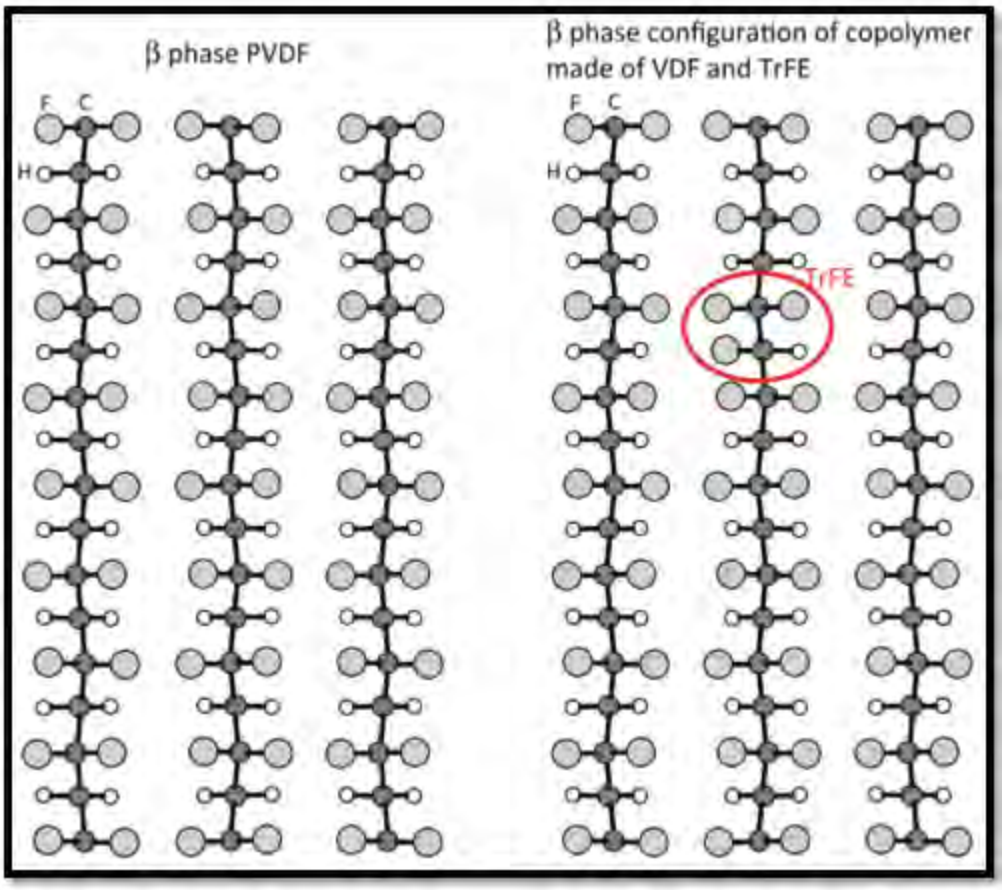

Fig: 1.12 Effect of steric hindrance on Beta phase [46]

1.8. PUND Measurement:

The PUND (Positive UP Negative Down) measurement is employed to determine the accurate value of the remnant polarization in ferroelectric materials. The apparent value of the remnant polarization may contain contributions from dielectric and space charge effects. However, the PUND technique calculates the true value of remnant polarization by eliminating the impact of these factors and only considers the polarization related to switching domains [47].

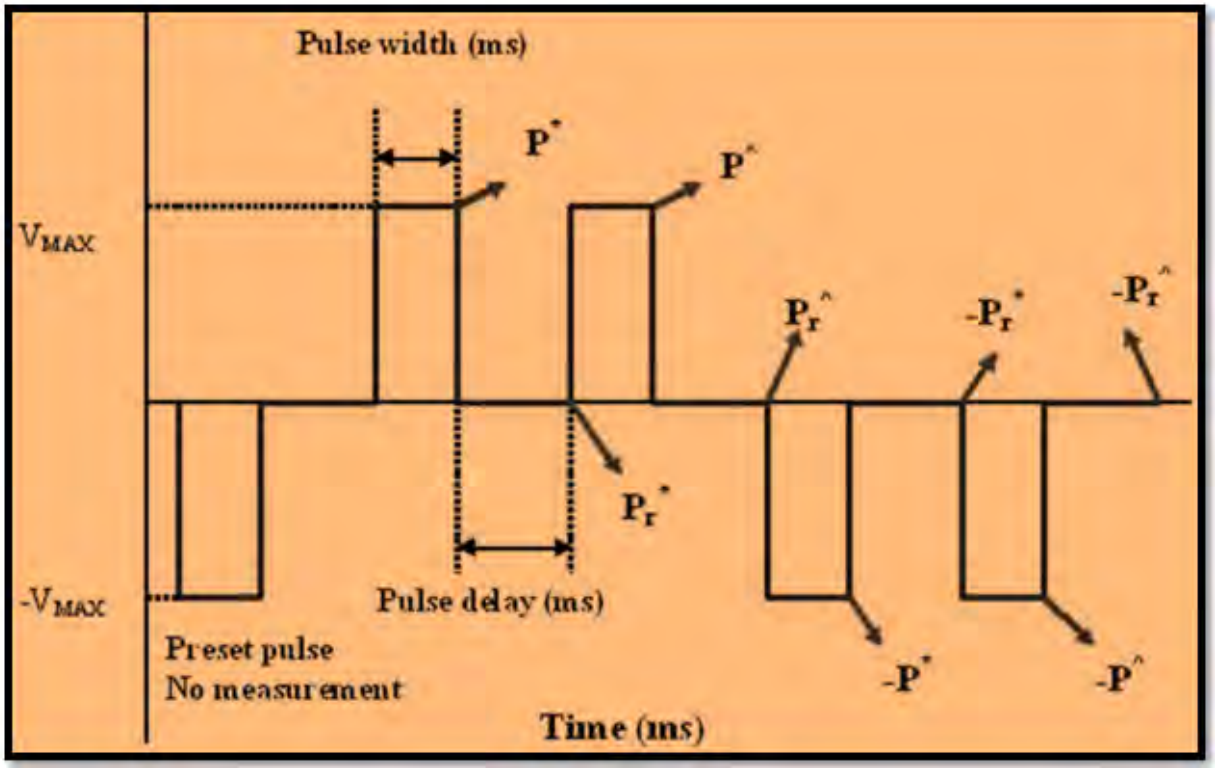

Fig: 1.13 Schematic illustration of PUND measurement [48]

Figure 1.13 shows PUND (Positive UP Negative Down) measurement technique, which requires subjecting the ferroelectric specimen to five pulses for a predetermined time interval, named as pulse width. Pulse delay is the time duration between each pulse. The pulse delay is required in order for the specimen to relax and stabilize the polarization before applying the next pulse. All five cycles are described below:

1) First Cycle: The first cycle in PUND measurement is to apply a negative voltage to the ferroelectric sample in order to polarize all dipoles in the opposite direction; this is called pre poling the sample. The voltage is then turned off letting the sample to relax. This process is essential for preparing the ferroelectric sample for the subsequent PUND measurement cycles.

2) Second Cycle: It is known as positive cycle and is used to align the dipoles in positive direction. In PUND, the positive pulse is utilized to calculate the contribution made by dipoles from the space charge, dielectric, and ferroelectric regions. The polarization is represented by P^*. After a specific time interval, that field is turned off. The device measures P_r^* during delay time.

3) Third Cycle: It requires applying voltage in the same direction as the positive cycle. It is called up cycle. Throughout this cycle, device measures the polarization, designated as $P^\wedge$. Following that, a resting phase is introduced in which the voltage is set to zero for a particular duration and the device measures polarization, designated as $P_r^\wedge$ within the ferroelectric material during this time.

4) Fourth Cycle: In this cycle voltage is applied in negative direction. The polarization is represented by - P^*. Soon after, the voltage is set to 0 volts and a time delay is given for a specific time interval. The instrument measures $-P_r^*$ during delay.

5) Fifth Cycle: In this cycle voltage is applied in the same manner as in the Negative cycle. This is referred to as the Down cycle. The instrument measures $-P^\wedge$ throughout this cycle. After a specific time delay, the voltage will be set to 0 volts. $-P_r^\wedge$ is measured by the device during this time delay.

Subtracting the polarization by the third (5th) pulse from the second (4th) pulse yields the true value of remnant polarization [47]. Figure 1.14 depicts the PUND loop obtained from PUND graph.

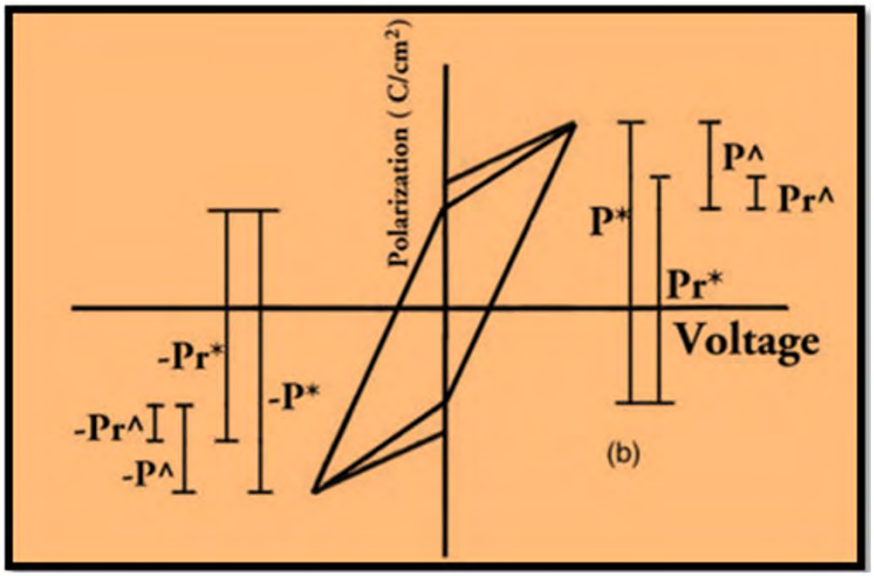

Fig: 1.14 PUND loop indicating the polarizations measured during each pulse [48]

1.9. Motivation:

The ferroelectric features of PVDF (Polyvinylidene fluoride) thin films and their high remnant polarization, have made them a subject of considerable interest [49]. PVDF contains four structural phases, known as Alpha, Beta, Gamma, and Delta. It is important to mention that the Beta phase exhibit significant ferroelectric characteristics [50]. This phase can be distinguished by the presence of monomers with all Tran's conformations (TTTT) and requires specific conditions to be attained [50]. A good strategy for obtaining the Beta phase of PVDF is to make a copolymer using TrFE (Trifluoroethylene), which may easily crystallize to this phase. PVDF-based polymers possess the characteristics of being semi-crystalline materials. They are extremely desirable due to their unique ability to give adjustable ferroelectric and piezoelectric characteristics. They have good mechanical properties, as well as significant chemical and thermal stability and high piezo and pyro coefficients, making them suitable for a wide range of applications such as sensors, detection systems, storage devices, and healthcare. Furthermore, for their use in electronic devices that are flexible, free-standing PVDF films or those formed on flexible substrates are very fascinating [51].

It is difficult to fabricate thin films on a conducting substrate that have strong adhesive characteristics while maintaining a ferroelectric phase. Creating a capacitor-like shape for appropriate testing of such samples demands careful handling and altering of the thin film specimens. As a result, P(VDF-TrFE) thin films have captured the interest of researchers due to their ability to achieve a voltage range adequate for operation. The aim of this research is to examine and fully understand the non-switching and switching characteristics for thin films fabricated from P(VDF-TrFE) using extensive ferroelectric tests. One goal of our research is to also look at how ferroelectric characteristics vary when two different electrode materials are deposited on PVDF-TrFE thin films. The ferroelectric loop has been examined on Pt and Ag-coated specimens.

Chapter 2 Characterizations and Techniques

The current chapter covers experimental methods and characterization techniques in detail that are used in synthesis and analysis respectively. A flow chart provides a quick summary of all techniques employed in the present work as shown in figure 2.1.

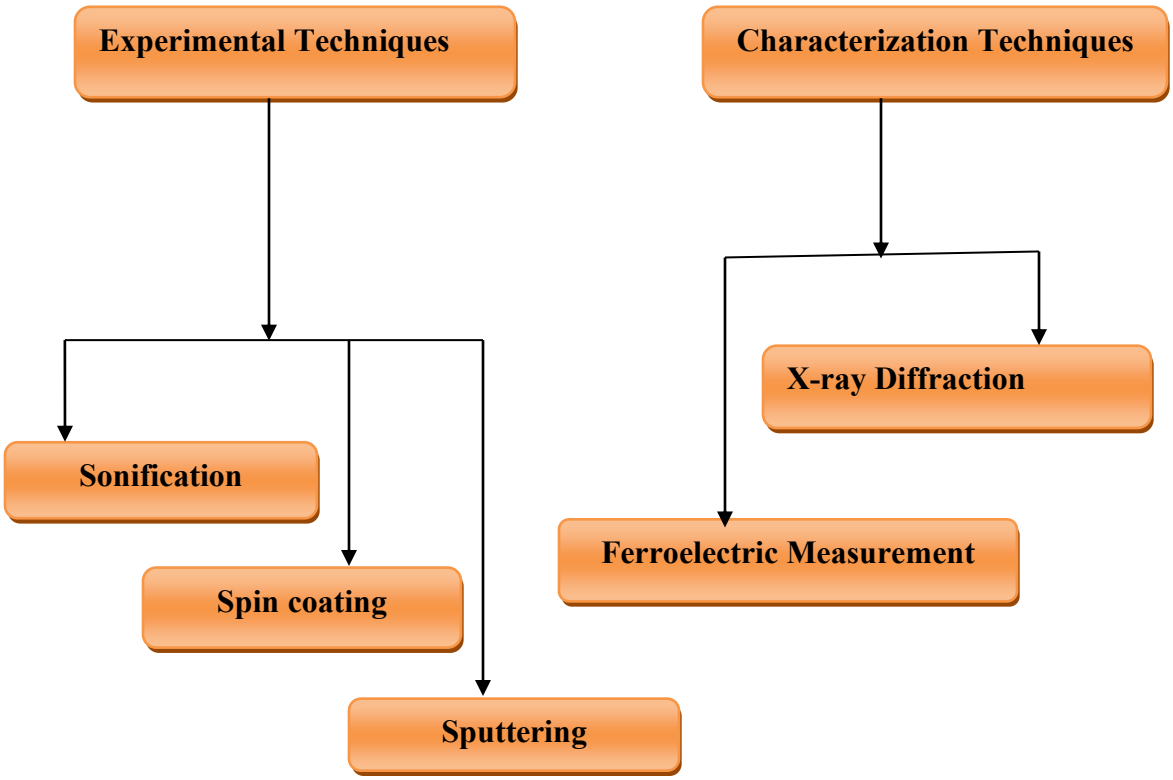

Fig: 2.1 Flow chart of experimental and characterization techniques

2.1. Spin Coating:

Spin coating refers to a technique that involves applying of a liquid solution to the middle of a flat substrate. The centrifugal force distributes the solution towards the outside when substrate rotates, resulting in thin and also uniform film throughout the surface [52]. A spin coater is a laboratory instrument used to perform this task. The following stages are involved in spin coating technique:

To ensure the appropriate adhesion of thin film, the substrate is cleaned. The solution has been prepared by dissolving the material to be spin coated in a suitable solvent.

2.1.1. Dispensing of Solution:

On the washed substrate's center, just a few drops of the solution are deposited by using a dropper. It may be deposited in two different ways:

1. Static Dispense: The process of depositing small quantity of the solution on an immovable substrate is commonly referred as static dispense. When dealing with solvents that are highly volatile static dispense might prove advantageous. However, if not correctly controlled, it can result in problems such as air that has been trapped in bubbles along with uneven thickness of film [53].

2. Dynamic Dispense: Dynamic dispense is the depositing of solution while substrate rotates at a slow rotational speed. This method is used because it wastes less solution [54]. Dynamic dispense may assist to achieve evenly distributed coatings by reducing the chance of confined air bubbles and offers greater control over thickness of film. However, greater control of dispense rate and rotation speed of substrate may be required to achieve optimal outcomes.

2.1.2. Spinning:

Centrifugal force spreads the solution uniformly throughout the surface after the spin coater device accelerates substrate. Depending on the intended thickness and uniformity of film, the process of spinning can be carried out at different speeds and time. It consists of three steps as follows:

- **Spin Up:** "Spin up" corresponds to the beginning phase of spinning procedure in which the substrate accelerates from a position of stillness to the intended rotational speed [55]. This phase is essential for producing a smooth and uniform thin layer on substrate**.**
- **Spin off**: When the substrate spins, solution is distributed from the middle of it to the corners. Some of the solution is removed from the substrate as it approaches towards edge by centrifugal force [55]. Spin off may assist to achieve uniform thin layer on desired substrate by removing surplus coating material.

2.1.3. Evaporation:

The solvent begins to evaporate when our substrate spins, leaving a thin layer of the substance on the entire surface [56].One layer of solution is obtained after drying for a suitable time. The previous actions will be reiterated to obtain desired film thickness [57].To enhance the film's adhesion and crystallinity soon after spin coating, the substrate may undergo further treatment process like thermal annealing.

2.1.4. Factors influencing film thickness:

Several factors may impact film thickness in spin coating procedure. Some of the factors are:

- **Speed of spin:** The substrate's rotational speed during whole process has a major influence on thickness of film. Greater speed causes solution to distribute more rapidly throughout surface, resulting in thinner films in general [58].
- **Time of spin:** The total time during spin coating procedure influences film thickness as well. Prolonged spin period results in thinner films because extra solution has been given longer time to be dropped off from the substrate [58].
- **Solute concentration**: The percentage of solute in the solution can affect film thickness. High concentration usually results in thicker films, whereas low concentrations result in thinner films.
- **Evaporation rate:** High rate of evaporation leads to thinner films because solvent evaporates faster during coating. Slow evaporation rate, on the other hand, can result in thicker films because solvent evaporates slowly, and solute had enough time for settling on substrate.
- **Viscosity of solution:** The viscosity of solution has a major impact on film thickness. Solution of high viscosity produce thicker films because they oppose spreading during spin coating [58].

We used an Ossila spin coater as depicted in figure 2.2. It has three main parts chunk, plug and keypad. The chunk has been designed for holding substrates. The keyboard can be used to change the rotation time frame and speed. It can be operated at rates between 120 and 6000 revolutions per minute. The display shows the spinning duration and speed settings.

Fig: 2.2 Ossila Spin Coater [59]

2.2. Sonifier:

For cleaning purposes, we used the Branson sonifier as shown in fig. 2.3.A sonifier is electronic equipment which transforms an electrical signal into mechanical to produce mechanical waves. There are three important components of sonifier. These are the horn, converter, and power source [60] .The power source transforms AC voltage in to electrical energy whose frequency is 20 kHz. In a converter, electrical energy is transformed into mechanical oscillation. Lead zirconate titanate serves as the electrostrictive component of the converter. It contracts and expands in response to an alternating voltage which is transmitted towards horn tip submerged in fluid. There are two operating settings for the Sonifier: continuous and pulsed. In a pulsed mode, a solution receives one pulse of ultrasonic waves per second. The range of this pulse time is 0.1 to 0.9 seconds. The Sonifier is adjusted for constant operation in continuous Mode. The user can regulate the duty cycle, amplitude, and time duration. The timer offers time intervals of 0 to 15 minutes. Duty cycle is controlled by a gauge that has a range of 10% to 90% per second. By rotating the output control in a clockwise orientation, the wave's amplitude can be adjusted [61] .

Fig: 2.3 Branson Sonifier [62]

2.3. Plasma Sputter Coater:

Sputter coating, a form of physical vapor deposition (PVD) technique, is used for coating thin layers of a material on a substrate using a specialized instrument called a plasma sputter coater [63]. The principle of sputtering is to bombard a target substance, usually a metal, with high-energy ions that are produced in plasma. As a result of the collision between these ions and the target substance, atoms are ejected from the target. Following their passage through vacuum cavity, the ejected atoms deposit on the substrate to develop a thin layer [64]. For sputtering purpose, we used the GSL-1100X-SPC-12 Compact Plasma Sputter Coater as depicted in figure 2.4. The main parts of sputter coater are vacuum chamber, substrate holder, target, needle valve, vacuum pump, power source and plasma creation system as shown in figure 2.5. A vacuum chamber is an enclosed cavity where the whole sputtering process is carried out in a controlled environment of vacuum. It is a component that holds our substrate in a suitable position in

reference to the particular target**.** It is the source substance that will be sputtered. We mount it on a holder for target**.** With the aid of a needle valve, the flow of gas can be regulated. It is used to establish vacuum environment inside the cavity. Direct current (DC) is usually used in plasma formation systems, which create plasma. It supplies power to plasma generation device.

Fig: 2.4 GSL-1100X-SPC-12 Compact Plasma Sputter Coater [65]

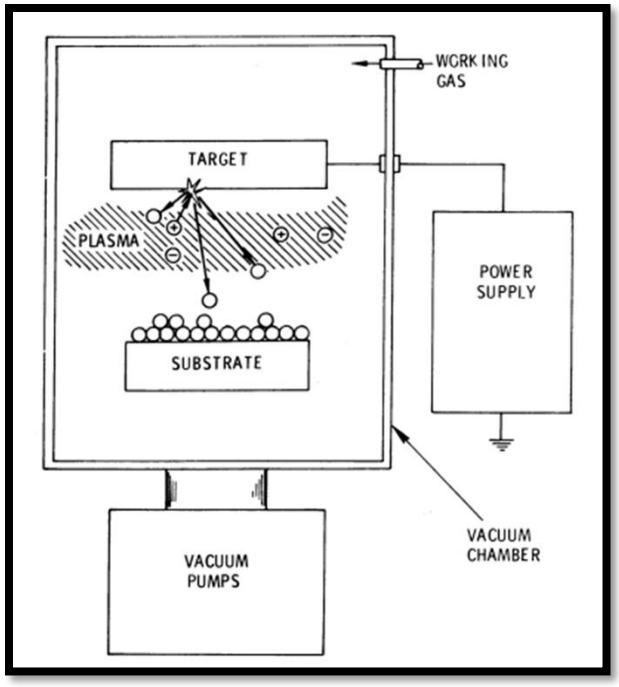

Fig: 2.5 Basic illustration of Sputtering technique [66]

2.4. X-ray Diffraction Technique:

X-ray diffraction is a tool used to identify the structure as well as the characteristics of materials that are crystalline. This process relies on the interactions of X-rays with atoms of crystal lattice. A diffraction pattern is produced when X-ray radiations strikes a crystal and the atoms of crystal diffract X-rays in different directions. Researchers can learn a lot about the structure of crystals by studying this pattern [67].

2.4.1. Generation of X-rays:

The tungsten filament is exposed to heat inside vacuum chamber to produce a beam of electrons. The electrons accelerated by the filament were directed towards a copper-based target material. This interaction results in a spectrum that includes both characteristic X-rays and continuous Bremsstrahlung radiation which is shown in Figure 2.6. Filters are introduced to eliminate undesired X-rays allowing just desired one K pass through. The selected X-rays are directed towards the sample which produces scattering pattern that reveals the structure of material [68].

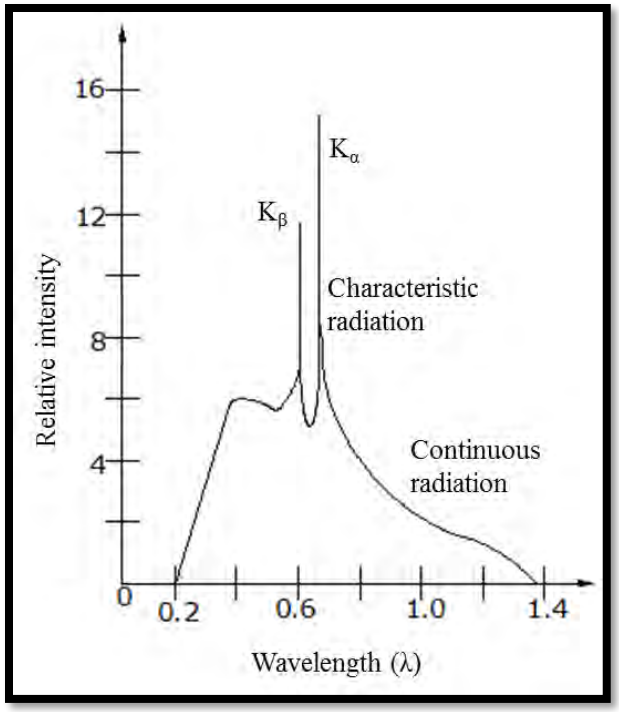

Fig: 2.6 Spectrum of X-ray radiation generated by target material [69]

2.4.2. Principle of XRD:

The principle of XRD is Bragg's Law. Bragg's Law describes the relationship between the interplanar spacing of a crystal lattice and the angles, at which its atoms scatter X-rays[70].Mathematically,

$$2d\sin\theta = n\lambda \quad (2.1)$$

Here, "n" is reflection order, "λ" is incident X-ray's wavelength, "d" is crystal's interplanar spacing, "θ" is the angle between the incoming X-ray and diffracting plane.

X-rays are dispersed in various directions when they interact with crystal lattice. When the waves that scatter are in phase, constructive interference takes place, producing a high intensity peak. This occurs when, according to Bragg's Law, the path difference between the dispersed rays is an integer multiple of the X-ray wavelength. Several bright spots, also referred as peaks, arranged in a distinctive pattern are produced by the incident X-rays on a crystal sample, creating a diffraction pattern. These peak's locations and intensities gives information of crystal structure [70]. Figure 2.7 shows diffraction of X-rays by crystals.

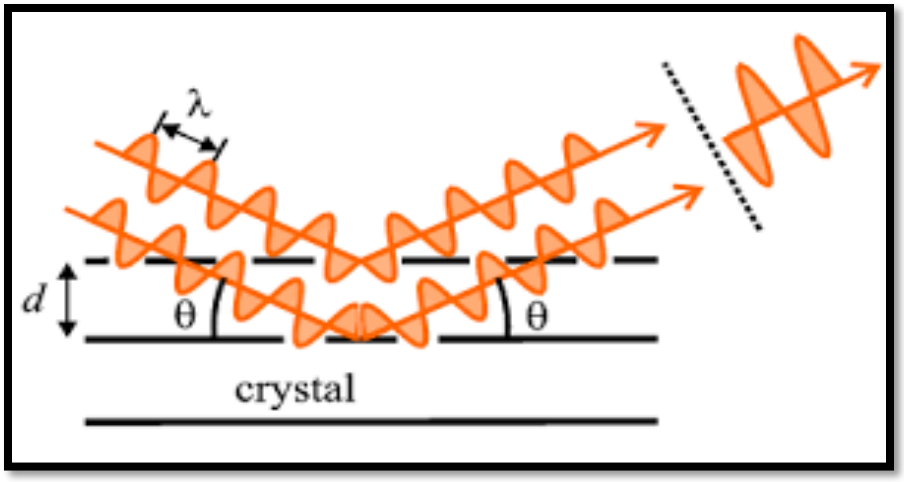

Fig: 2.7 Principle of X-ray Diffraction [71]

We use PANalytical Empyrean Setup to examine the structure of the PVDF-TrFE thin film as shown in figure 2.8. A target substance, typically copper, is bombarded with electrons that are highly energetic by X-ray source. This leads the target to emit K-alpha radiation, or X-rays. The sample is placed on sample holder. To guarantee reliable dispersion data, the object being studied must be correctly oriented with the incoming X-ray radiation. The sample will be exposed to an incoming X-ray beam and a detector detects the diffracted X-rays. To ensure that all Bragg reflections are recorded, the sample as well as detector undergoes rotation to examine a variety of diffraction angles. Detector records intensity of scattered X-rays as a function of 2theta angle. The resulting information is a collection of peaks which includes details about the specimen's structure and the dimensions of the unit cells. Special software's are used to analyze diffraction pattern.

Fig: 2.8 PANalytical Empyrean Setup

2.5 Ferroelectric Measurement:

The Polarization-Electric Field ($P-E$) Hysteresis Loop and PUND were measured using the principle of Sawyer Tower circuit for determining a material's ferroelectric characteristics. For ferroelectric analysis, we used the PolyK Polarization Loop set up as shown in figure 2.9.

Fig: 2.9 PolyK Polarization Loop and Dielectric Breakdown Setup [72]

2.3.1 Sawyer Tower Circuit:

In 1930, C. H. Sawyer and C. H. Tower designed the Sawyer Tower Circuit for studying the properties of ferroelectric crystals. The polarization of ferroelectric material varies, depending on the electric field when a voltage is applied to it. In order to determine the ferroelectric characteristics of substance, this includes coercive field, remnant polarization and saturation polarization, the Sawyer Tower Circuit records these variations and gives a P-E hysteresis loop. Voltage source, resistor, sample capacitor, reference capacitor (C_R), and data plotter are the fundamental parts of a Sawyer Tower Circuit. The ferroelectric specimen is a thin film in our case. A sinusoidal voltage signal V is given to the ferroelectric sample. The voltage applied to the ferroelectric capacitor needs to be high enough to cause polarization saturation [73].

Typically, a reference capacitor (C_R) and a sample capacitor (C_S) are linked in series with the voltage supplier. By comparing the voltages, reference capacitor enables the measurement of polarization. To show the $P - E$ hysteresis loop, the output is sent to a data plotter. The plotter creates a graph that displays the material's ferroelectric characteristics by plotting the electric field (E) on the x-axis and the polarization (P) on the y-axis. Figure 2.10 shows schematic illustration of Sawyer Tower Circuit.

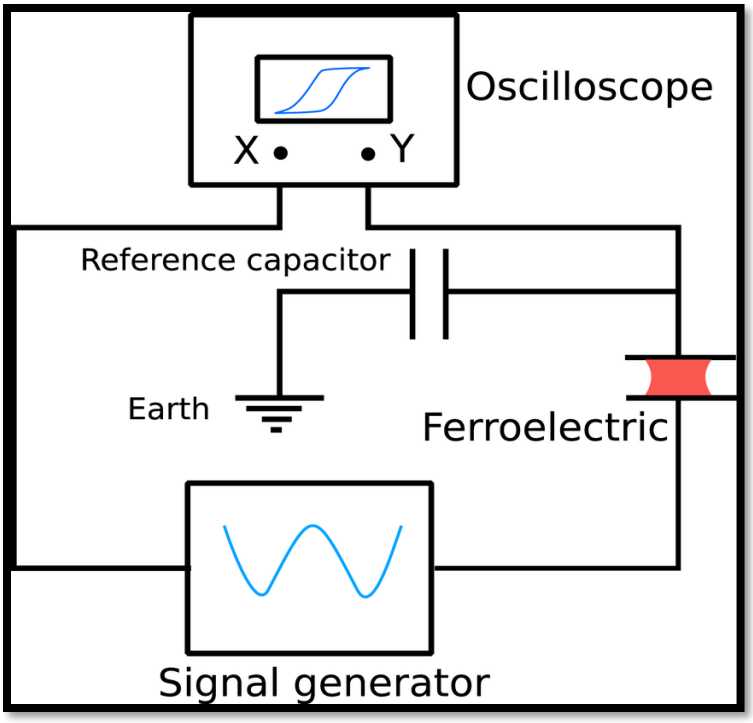

Fig: 2.10 Schematic illustration of Sawyer Tower circuit [74]

Chapter 3 Synthesis and Characterization

This chapter explains the fabrication of P(VDF-TrFE)/Pt and P(VDF-TrFE)/Ag thin films deposited on ITO coated glass substrate and detailed structural analysis.

3.1. Thin film fabrication:

Fig: 3.1 show overview of the fabrication method.

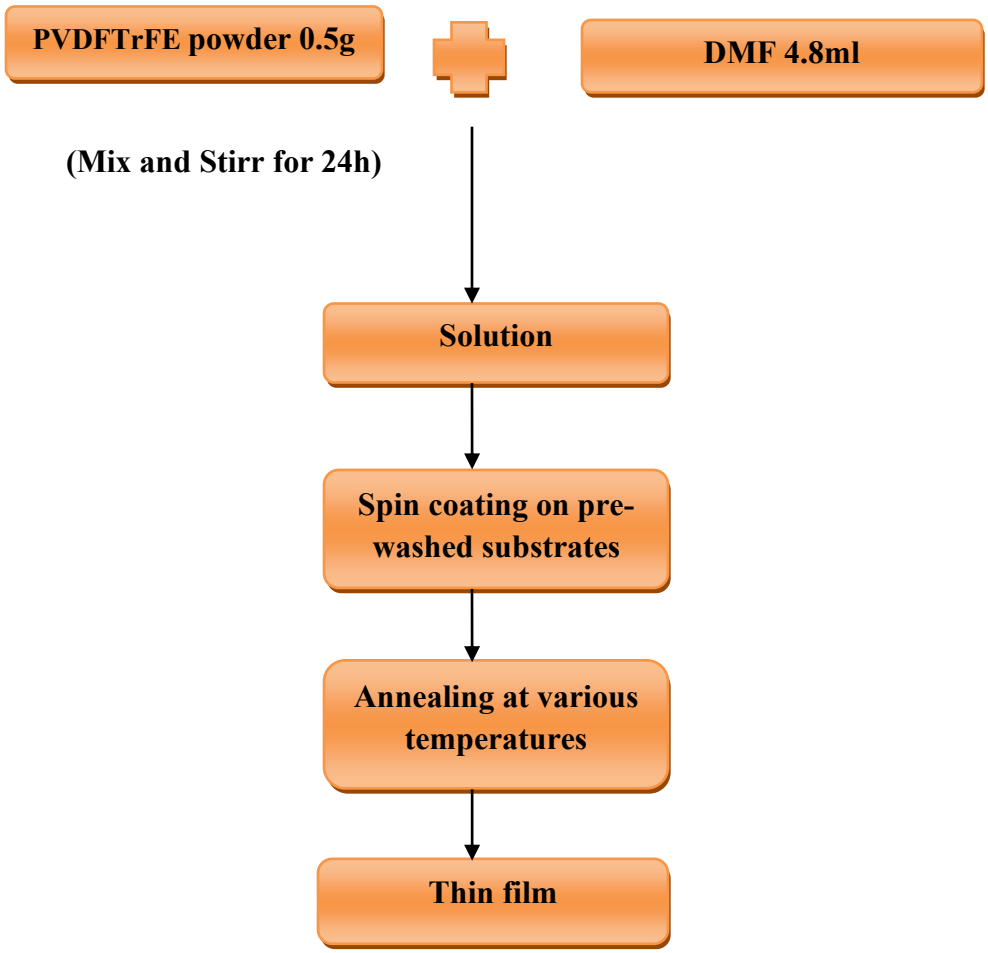

Fig: 3.1 Overview of thin film fabrication

3.1.1. Substrates Cleaning:

The substrates were cleaned using a Branson sonifier as shown in figure 3.2. Initially the conductive surface of substrate is examined using a multimeter. A beep sound will be produced by connection on conductive surface. We used ITO-coated glass substrates. Substrate is then placed in a propanol-filled beaker such that its conductive surface was exposed to horn point for efficient cleaning. The beaker is positioned so that the horn point is properly immersed in the fluid. The timer is fixed to 10 min. The sonifier produces ultrasound waves of suitable speed and amplitude for given duration of 10mins.After that substrate is placed in Hellmanex water and DI water following the same procedure for the duration of 10 minutes in each.

Fig: 3.2 Substrate cleaning

3.1.2. Solution preparation:

For the solution preparation, calculated quantity of 10wt% of P(VDF-TrFE) and solvent (DMF) were weighed. After that both were mixed vigorously at hot plate. During stirring, the resulting mixture was heated to 60 °C for one hour and then maintained at room temperature for 24 hours. The preparation of solution is shown in figure 3.3.

Fig: 3.3 Preparation of solution

3.1.3. Spin Coating:

At 2000 rpm and for 30s, solution was spin coated onto an ITO-coated glass substrate and dried on pre-heated hot plate at 80°C for 10 minutes. To produce the desired number of layers, this method was performed 2 and 4 times, respectively. In order to improve crystallinity, films were eventually annealed[75] for a duration of three hours at 110°C, 120°C,130°C,140°C and 150°C respectively . Figure 3.4 provides an overview of the spin coating method for film deposition and annealing.

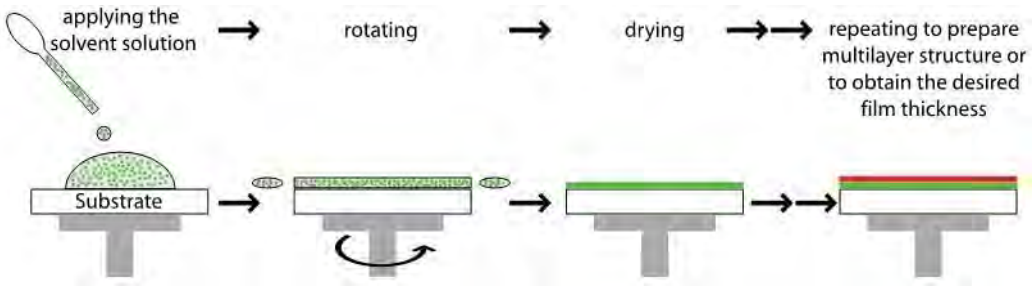

Fig: 3.4 Spin Coating [76]

3.1.4. Sputtering:

Utilizing a plasma sputter coater, top electrodes of platinum and silver were grown by using a shadow mask with a diameter of about 200 mm. We set gas pressure to be 10 Pa and adjust current at 10 mA. Sputtering duration for a single layer has been set to be one minute, with a five-minute gap between each consecutive layer. Figure 3.5 provides a schematic representation of sputtering.

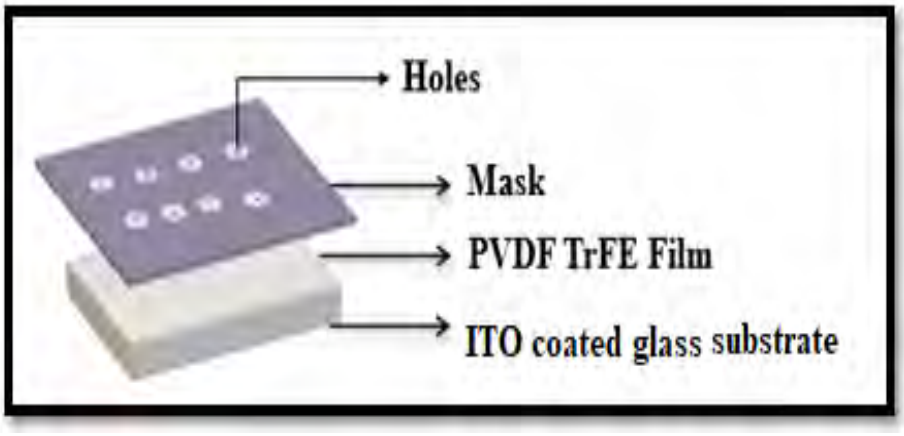

Fig: 3.5 Schematic illustration of electrodes deposition

3.2. X ray Diffraction Pattern:

Figure 3.6 shows the diffraction pattern of X-rays of thin films annealed at 110°C, 120°C, 130°C, 140°C, and 150°C. The presence of a peak at 19.7 degrees indicates the presence of the Beta phase of P(VDF-TrFE), which is consistent with previous research [77].Reflection at 19.7degrees represent Bragg diffraction of (110)/(200) whereas the reflection at 30.2 degrees and 35.3 degrees are from diffraction of (222) and (400) planes [78].

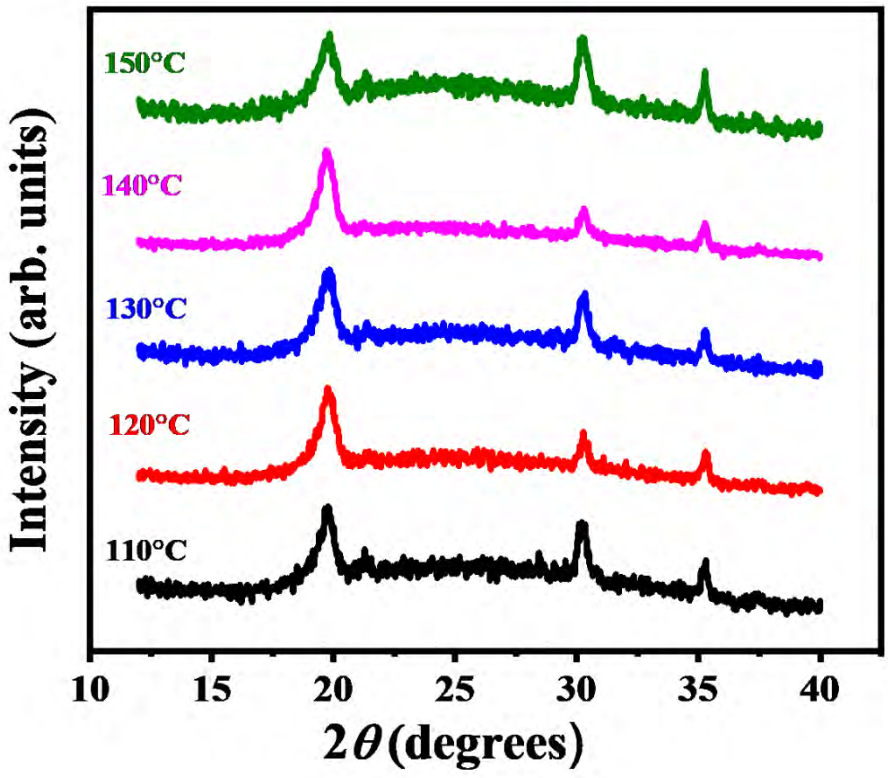

Fig: 3.6 XRD pattern of P (VDF-TrFE) thin films annealed at 110°C, 120°C, 130°C, 140°C, and 150°C deposited on ITO coated glass.

The major peaks of P(VDF-TrFE) are de convoluted to obtain their amorphous and crystalline portions. Figure 3.7 depicts the deconvoluted peaks. The following formulas are used to compute the percentages of crystalline and amorphous regions:

$$\%X_A = \frac{A}{A+C} \times 100$$

Whereas X_A denotes percentage of the amorphous region. Also, A and C denote the corresponding amorphous and crystalline area.

Similarly, the percentage of crystalline portion is calculated by:

$$\%X_C = \frac{C}{A+C} \times 100$$

Here X_C denotes percentage of the crystallinity.

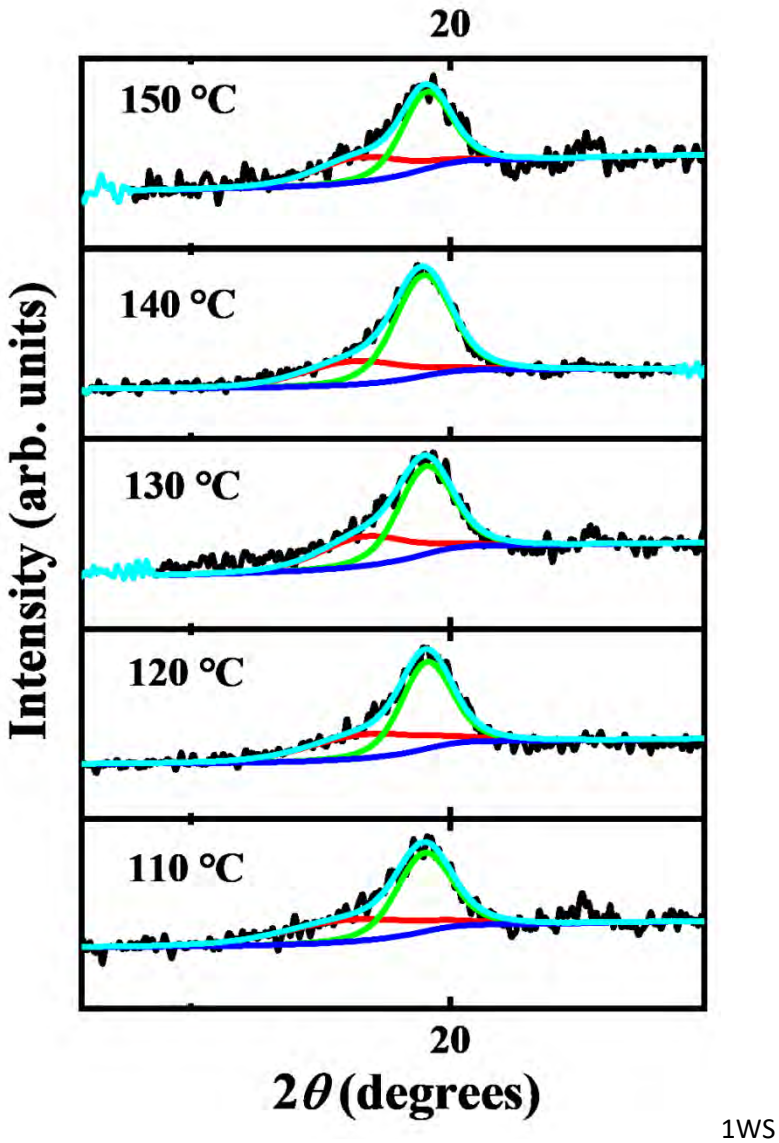

1WS

Fig: 3.7 Deconvoluted peaks for P(VDF-TrFE) films annealed at 110°C, 120°C, 130°C, 140°C, and 150°C deposited on ITO coated glass

Crystalline and amorphous percentages for samples with different annealing temperature are presented in table 3.1. 110°C, 120°C, 130°C, 140°C and 150°C represents the samples annealed at five different annealing temperatures of P(VDF-TrFE) solution. We observe that amorphous region rises, and the crystalline region reduces as the annealing temperature decreases. It could be caused by a strain mismatch between crystallites in the films, which prevents crystallization [26]. The percentage of crystallinity for beta phase gradually increases as the annealing temperature increase from 110°C to 140°C, indicating enhanced crystallization of films at higher annealing temperatures. But as the annealing temperature goes near and above the melting point, the percentage of crystallinity falls, showing the existence of an ideal annealing temperature range for film crystallization [77].

Table 3.1 Percentage of amorphous and crystalline regions in P (VDF-TrFE) thin films annealed at 110°C, 120°C, 130°C, 140°C and 150°C

Sample	**Area Amorphous**	**Area Crystalline**	$\%X_A$	$\%X_C$
110°C	0.226	0.3469	39.44	60.56
120°C	0.2145	0.3525	37.83	62.17
130°C	0.1962	0.368	34.77	65.23
140°C	0.1868	0.46	28.88	71.12
150°C	0.1556	0.2721	36.38	63.62

In literature AFM image revealed information about surface morphologies of the materials. The substrate's AFM image displays a surface that is smooth with no grains. The unannealed sample's AFM image shows existence of numerous small grains on surface. The grains are around 10 nm wide and 20 nm long on average. The sample that is unannealed has a rough morphology. The grains on surface appeared orderly and tightly packed at annealing temperature of 120°C and they are 40 nm wide and 80 nm long. The size of grain gradually became larger as annealing temperature raised. The grain size for sample annealed at 140°C reached up to 120 nm in width and 210 nm in length. This suggests that annealing method aided in the formation of bigger crystalline domains inside copolymer film. When temperature

is 148°C the grains becomes enlarged further and neighbor grains joined to form 150 nm wide and 700 nm long rods [79]. Other scholars have also reported on the phenomenon of rod formation and grain coalescence [80]. At annealing temperature of 150°C the specimen's morphology changes, which leads to a decrease in the crystallinity.

The X-ray diffraction pattern of P(VDF-TrFE) films fabricated from simple and distilled DMF is shown in fig 3.8. When distilled DMF is compared with simple DMF, distilled DMF has more distinct along with well-defined peak based on the observed data. The sharper peak implies fewer impurities present in sample made from distilled DMF. Distillation is an extra purification procedure that helps to eliminate contaminants. The decision to choose between distilled or simple DMF is determined by the application along with the amount of purity required. For sensitive applications in which impurities may hamper intended result distilled DMF can be preferable. Simple DMF, on the other hand, may be acceptable as well as cost-effective in few critical applications wherein the existence of contaminants is not major concern [81]. Fig 3.9 shows deconvoluted peaks for P(VDF-TrFE) films fabricated from simple and distilled DMF.

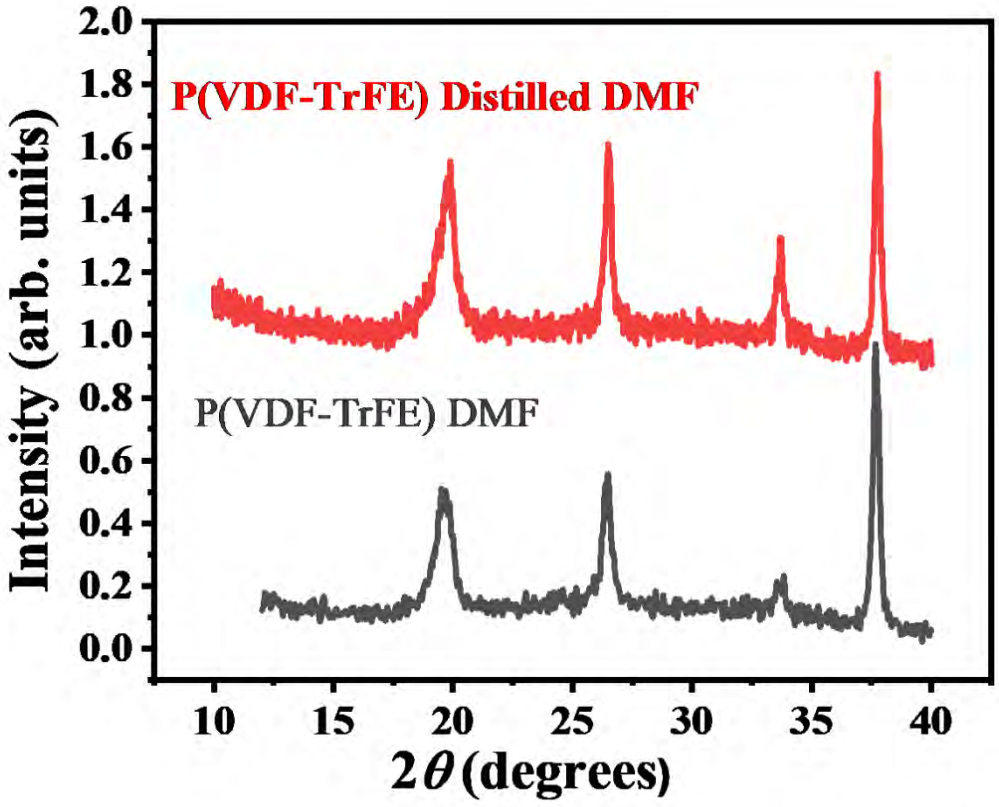

Fig: 3.8 XRD patterns of P(VDF-TrFE) films fabricated from simple and distilled DMF

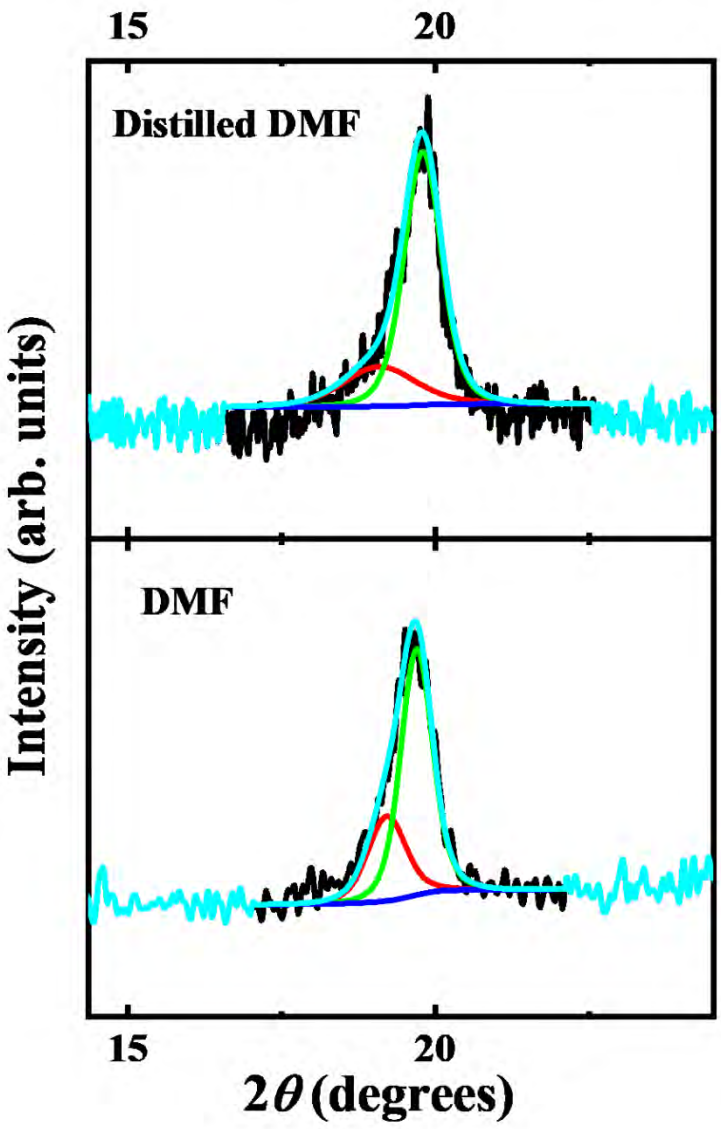

Fig: 3.9 Deconvoluted peaks for P(VDF-TrFE) films fabricated from simple and distilled DMF

Crystalline and amorphous percentages for samples fabricated from simple and distilled DMF are presented in table 3.2. Moreover, DMF that has been distilled has a higher crystallinity region than simple DMF due to fewer amounts of impurities present in it.

Table 3.2 Percentage of amorphous and crystalline regions in P (VDF-TrFE) thin films fabricated from simple and distilled DMF

DMF type	Area Amorphous	Area Crystalline	% X_A	% X_C
Simple	0.1016	0.248	29.06	70.93
Distilled	0.1041	0.3454	23.15	76.85

Chapter 4 Results and Discussion

The ferroelectric characteristics of thin films (annealed at different temperatures) of P(VDF-TrFE) deposited on ITO coated glass are examined in this chapter. The primary goal is to investigate the switching and non-switching behavior of films. Further, the capacitor like geometry fabricated with different metal electrodes is also analyzed.

4.1. P(VDF-TrFE) thin film ferroelectric characteristics:

Ferroelectric characteristics of 2L films annealed at 120°C,140°C and 150°C were analyzed to determine the ferroelectric switching behavior of P(VDF-TrFE) thin films. 2L corresponds to the thin films synthesized by spin coating and comprised 2 layers coated one by one at 2000rpm for 30 seconds respectively. The loops were recorded at room temperature with the applied voltage of 196V. The following sections are presenting the ferroelectric characteristics of these thin films in detail.

4.1.1. Variation of polarization at same voltage with different annealing temperatures:

Polarization behavior with the application of electric field has been examined through measurements of ferroelectric loops for P(VDF-TrFE) films annealed at 120°C, 140°C and 150°C temperatures. These loops were measured at 196V and at 10Hz. At room temperature, all samples displayed good ferroelectric loops, revealing the presence of switching polarization. Figure 4.1 depicts the ferroelectric loops annealed at different temperatures. All thin films withstand voltages up to 196V.

An ideal ferroelectric loop would be rectangular in shape, exhibiting sharp transitions among polarization states. The switching speed is uniform throughout all domains. However, the loops of ferroelectric materials can often be rounded and asymmetric thus deviate from their ideal behavior. The inhomogeneities existing in the sample are responsible for roundness in the ferroelectric hysteresis loops. Such inhomogeneities might be caused by impurities and defects present inside the material. When the material is subjected to an external field, some domains start to switch at first, whereas some domains remained unchanged. As the field increases, further domains switch till all the domains present in material reverse their

polarization. However, due to distribution in switching rates throughout the domains, the switching proceeds gradually instead of sharp transition [82].

Ferroelectric loops for thin films annealed at 120°C, 140°C and 150°C temperatures show an asymmetric effect with respect to polarization axis. Asymmetric loop refers to the loop in which there exists a variation in magnitude of positive and negative remnant and saturation polarization. Different factors that contribute to this asymmetric behavior of loops, which involves differences in interface between the electrodes and existence of polarity dependent leakage current. When we apply field to ferroelectric sample, charges accumulate at electrode interface, which creates potential barrier [83]. The barrier's height could vary among negative and positive polarization states because of the differences in interface traits. As a result of the difference in saturation and remnant polarization, the loop vertically shifts. Furthermore, asymmetry in contacts might cause polarity dependent leakage current [84]. If we apply field to ferroelectric substance, some current travels through interfaces rather than ferroelectric substance. The quantity of current flowing through the interfaces can be affected by polarity of field, which leads to difference in saturation and remnant polarization for negative and positive polarizations [85].

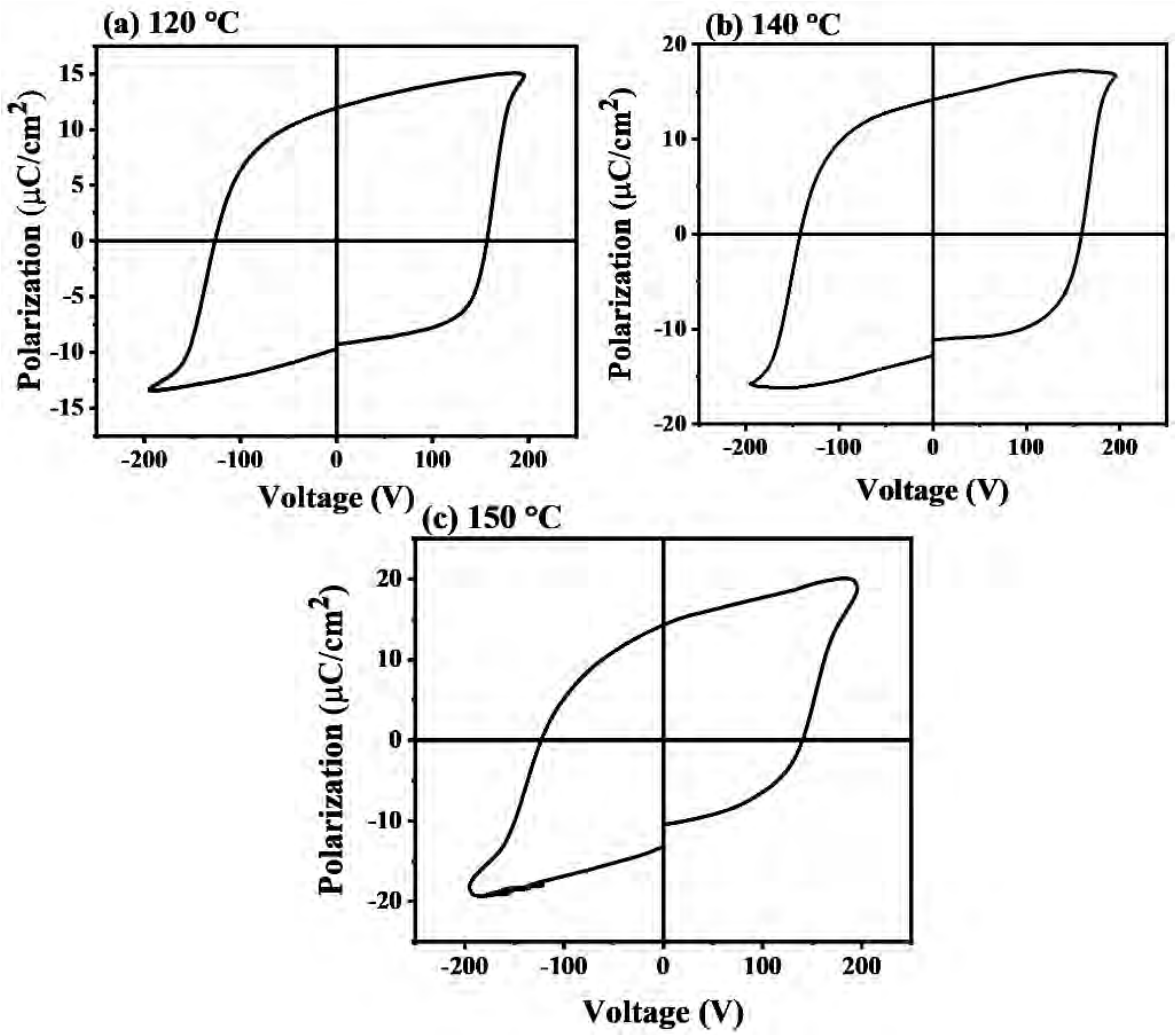

Fig: 4.1 Ferroelectric loops of P(VDF-TrFE) thin films annealed at (a) 120°C, (b) 140°C and (c) 150°C temperatures.

A distribution in switching speed may exist, as evidenced by current density vs. voltage plots illustrated in figure 4.2. The field applied to ferroelectric substance around coercive field, causes polarization to change and current travels across the material. Current density measures how much current flow per unit area. Current density plot for ferroelectric materials shows a peak around coercive field. The peak denotes point where the material's polarization direction is switched. Domain movement costs energy and resulting in a rise in current density at coercive field. The presence of several switching fields is revealed by broad peaks. However, magnitude of current density decreases and peak broadening increases with annealing temperature. The rise in crystallinity may enhance the ferroelectric characteristics of P(VDF-TrFE) thin films. When compared with amorphous regions, crystalline regions often

have an increased amount of order plus fewer defects [86]. This corresponds to the larger crystallite size and hence, greater movement of switching dipoles.

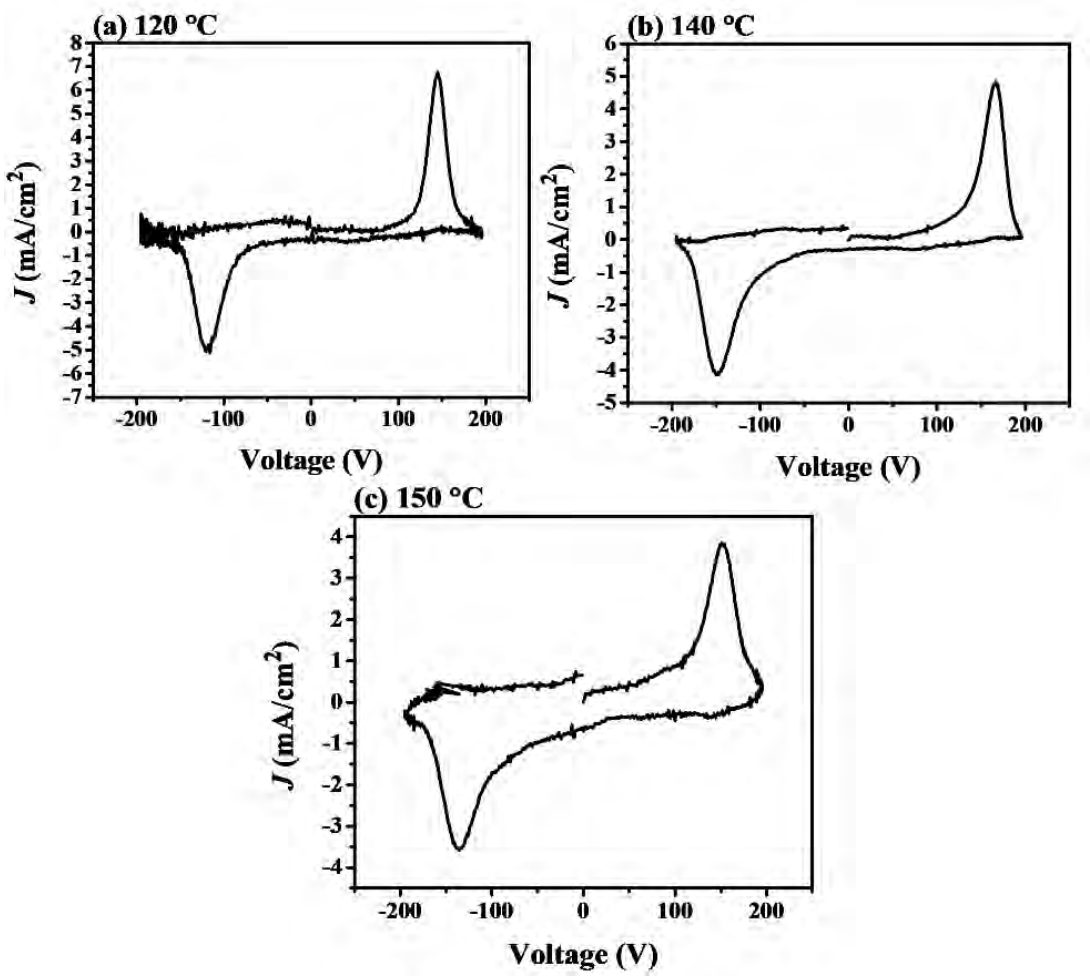

Fig: 4.2 Current density plots of P(VDF-TrFE) thin films annealed at (a) 120°C, (b) 140°C and (c) 150°C temperatures.

The hysteresis loops for P(VDF-TrFE) thin films that were annealed at different crystallization temperatures are shown in figure 4.3 and figure 4.4 shows enlarged view of rectangular portion of comparison of loops. The loops of these films were measured at 10Hz. Remnant polarization is observed highest at 150°C and lowest for 120°C. It shows a direct relationship between remnant polarization and annealing temperature at the same voltage. This result is consistent with those published in the existing literature [87]. The remnant polarization derived from hysteresis loop comprises contributions from multiple sources. These sources are polarization due to switching domains, polarization associated with

electrical conductivity and dielectric polarization. Electrical conductivity within the films can cause current to flow, which is commonly referred to leakage current. The leakage current may add to total remnant polarization. This current's magnitude is affected by the strength of applied field to ferroelectric substance. The presence of switching domains might have a considerable impact on remnant polarization measurements. The polarization which develops within a material because of alignment among dipoles due to applied field is known as dielectric polarization. This polarization may also contribute to the remnant polarization in ferroelectric substances. Dielectric polarization's magnitude is affected by the shape and frequency of applied signal. As a consequence, the polarization derived by loop does not offer information regarding the sample's true polarization, that is associated with switching domains, and is hence referred to as apparent remnant polarization [88].

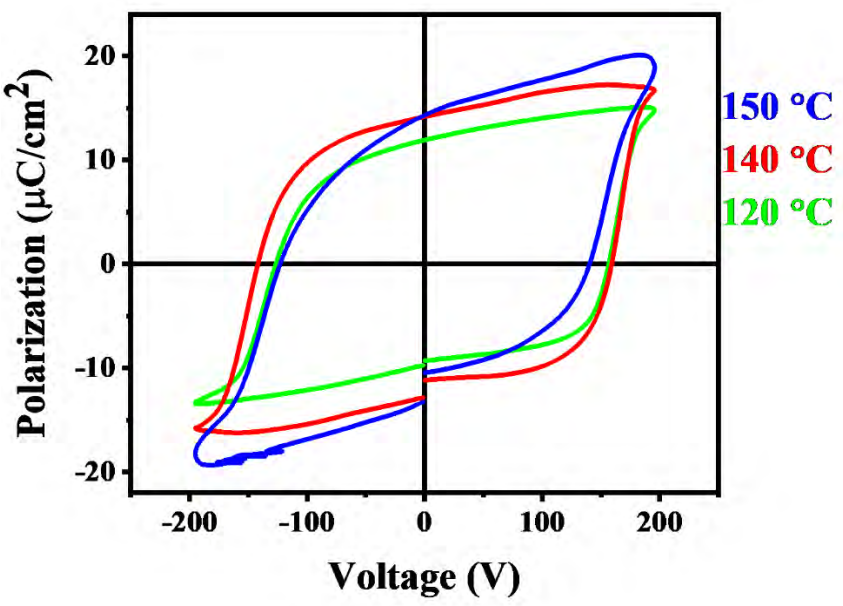

Fig: 4.3 Hysteresis loop exhibited by films annealed at 120°C, 140°C and 150°C

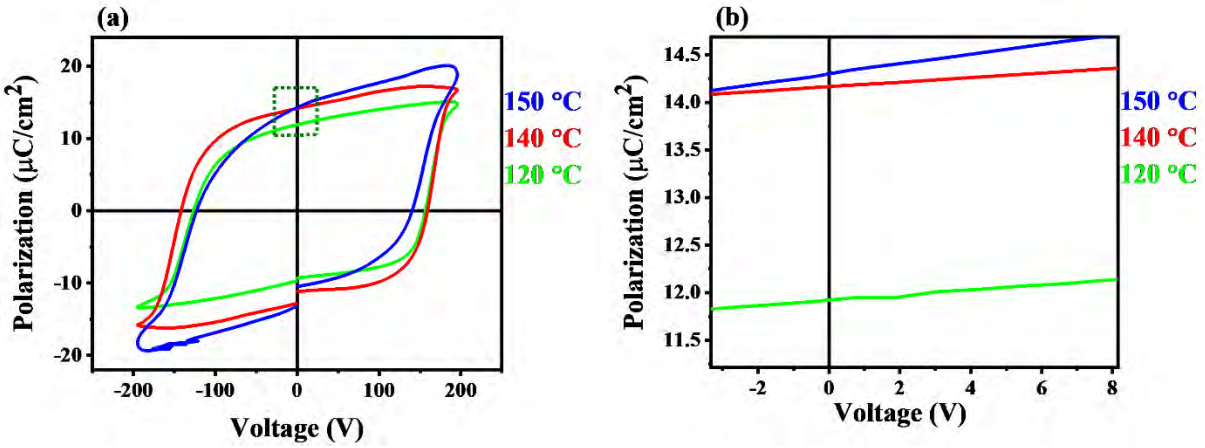

Fig: 4.4 Hysteresis loop (a) rectangular portion (b) enlarged view of rectangular portion

The apparent polarization's trend as a function of annealing temperature is shown in figure 4.5. The remnant polarization of P(VDF-TrFE) thin films whose annealing temperature is 120, 140, and 150°C was approximately 11.88, 14.15 and 14.31 μC/cm^2 respectively. The remnant polarization of films annealed at 140°C, and 150°C is higher than those annealed at 120°C, and this was attributed to β-phase crystallinity that occurred in P(VDF-TrFE) thin films based on crystallization temperature [89]. The remnant polarization increases with annealing temperature, reaching a maximum of 14.31 μC/cm^2 at 150°C. This increase in remnant polarization of thin films as one increases annealing temperature is consistent with various other papers [87]. However, as annealing temperature rises above melting temperature, crystallinity decreases, indicating the existence of optimum annealing temperature range for crystallization of copolymer films [90]. Since 150°C is close to melting temperature, crystallinity declines after this temperature [91]. Other studies also show that when annealing temperature is greater than melting temperature the ferroelectric characteristic for P(VDF-TrFE) films degrades [92].

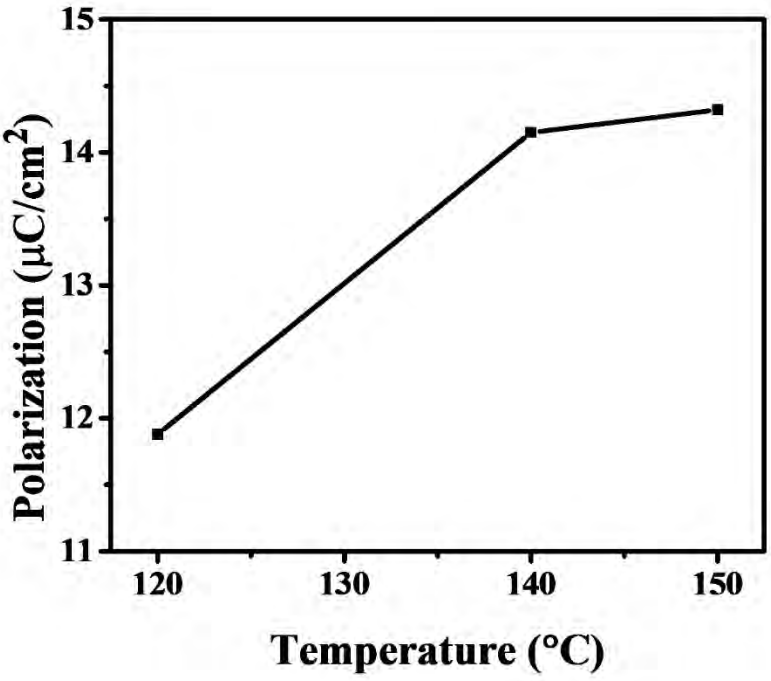

Fig: 4.5 Trend of apparent polarization as a function of annealing temperature

4.1.2. PUND measurement:

Positive-Up-Negative-Down (PUND) measuring technique was used to examine the sample's ferroelectric behavior. Using a voltage of 196V, square wave having 10ms of pulse width was applied. The pulse delay was set to be 1000ms. Figure 4.6 shows the resulting PUND graphs. The respective PUND loops are shown in fig 4.7. It The polarization in the positive (2nd) as well as negative (4th) cycles was caused by ferroelectric and non-ferroelectric components. Whereas polarization in up (3rd) and down (5th) cycles were caused by non-ferroelectric components. The values of polarization in 2nd and 3rd cycles of a perfect resistor will remain almost identical in positive direction, and similarly the values of polarization in 4th and 5th cycles in negative direction. However, we observed a considerable difference in polarization in both the 2nd and 3rd cycles in the PUND graphs, indicating the existence of a positive switching polarization. In a similar way a variation was found among the 4th and 5th cycles, indicating the existence of negative switching polarization. The difference indicates the presence of ferroelectricity in prepared specimens. As a result, the samples have switching domains which indicate ferroelectric behavior [11].

All non-ferroelectric characteristics in PUND measurements represent polarization which is not associated with the ferroelectric characteristic of specimens. These contributions may arise due to two major sources: leakage current and dielectric polarization [93]. Leakage current indicates flow of constant current across specimen even when applied voltage is constant. It arises because of material defects including contaminants, boundaries of grains, and surface effects. These defects can result in unintended conductive paths, allowing current to flow. Defects and crystalline/amorphous boundary contribute to space charge polarization within thin films of P(VDF-TrFE) [94]. To extract the switching domains contribution true polarization was calculated by deducting P (non-ferroelectric) from P (ferroelectric + non-ferroelectric) [95]. This yields $2P_r$ that is then divided with 2 to calculate the sample's true value of remnant polarization [96].

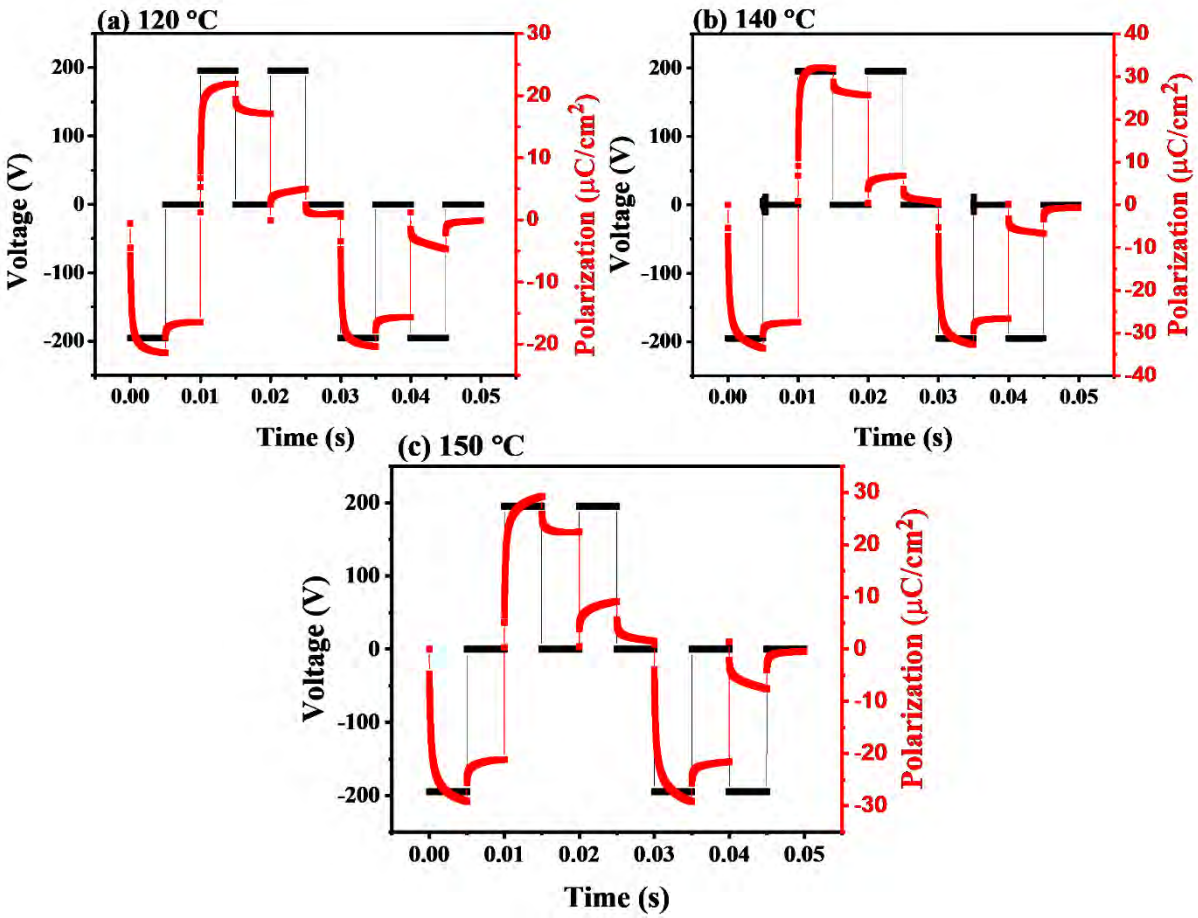

Fig: 4.6 PUND graphs of P(VDF-TrFE) thin films annealed at (a) 120°C, (b) 140°C and (c) 150°C

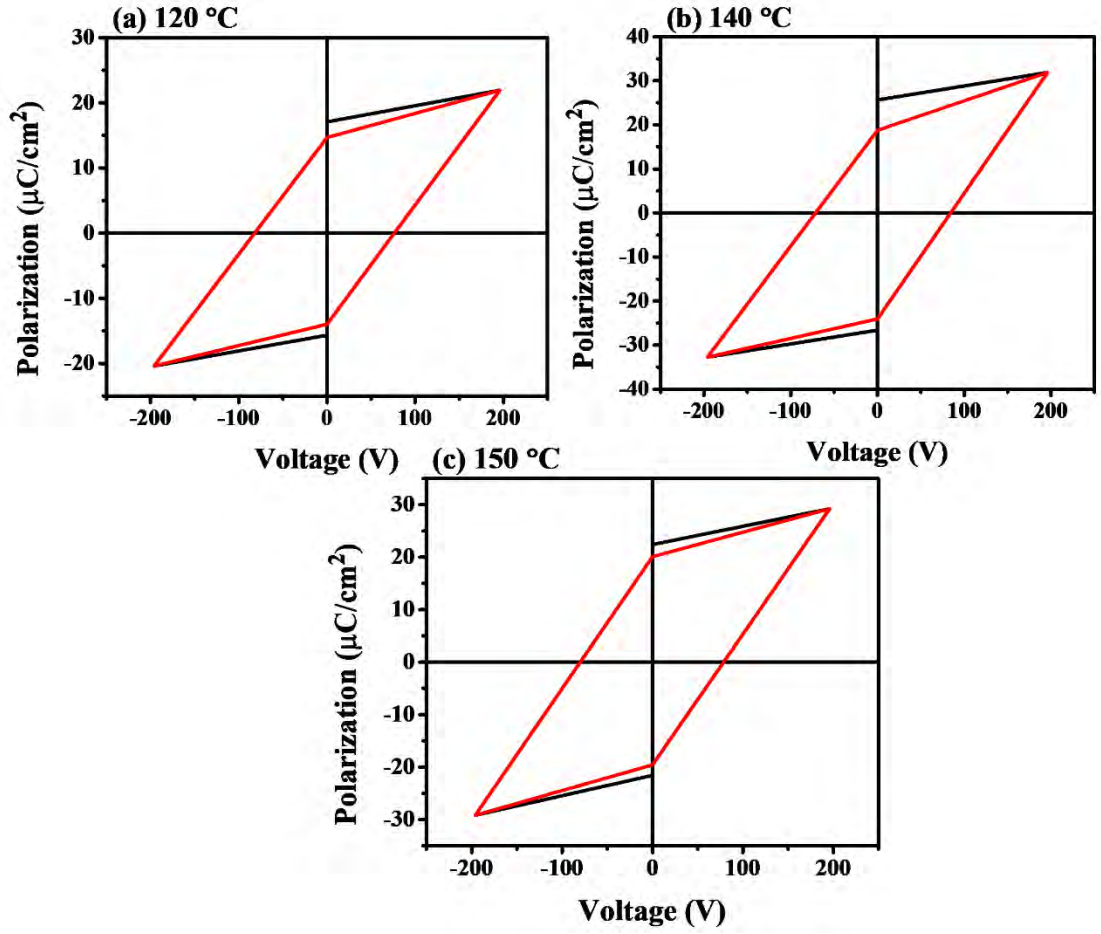

Fig: 4.7 PUND ferroelectric loops extracted from PUND graphs

Figure 4.8 depicts the true values of remnant polarization in samples with different annealing temperatures. At the same voltage, true remnant polarization is observed to be maximal for 140°C and least for 120°C. This demonstrates a direct relationship among true polarization and annealing up to an optimal temperature [77]. True value of polarization is ferroelectric characteristic of the sample [97]. The true value of remnant polarization is connected with polarization associated with switching domains [98]. The sample's ferroelectric characteristics are determined by the amount of crystalline portion [99]. The unannealed specimen's AFM image revealed the existence of numerous tiny grains on surface. The grains on surface grew more orderly and closely packed after annealing at 120°C. The size of grains increased on average. This indicated that annealing assisted in the development of bigger crystalline domains inside copolymer film. At annealing temperature of 140°C the size of grains further increased. This suggests that greater temperatures aided in the

formation and growth of crystalline domains. At 148°C the grains grew even bigger, and the neighboring grains began to combine resulting in structures that are elongated rod-like [79]. Other researchers have already documented the phenomenon of grain coalescence and rod formation which supports these findings [80]. Because of the change in morphology at 150°C, crystallinity decreases, and thus the true value of polarization drops.

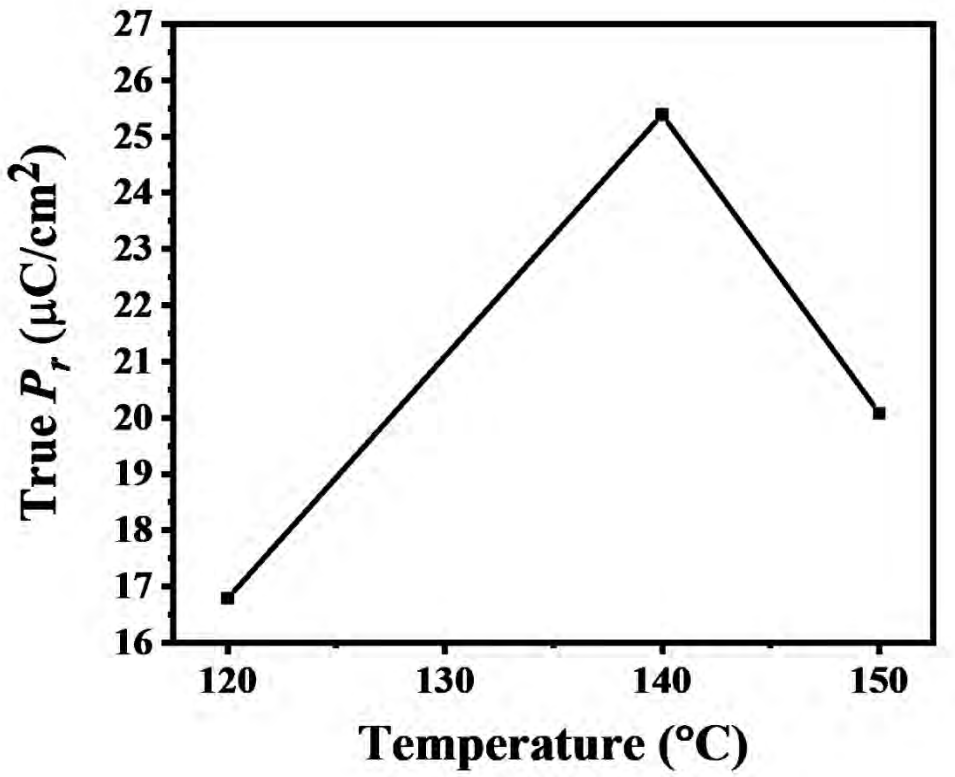

Fig: 4.8 True remnant polarizations vs. annealing temperature at 196V

4.1.3. Comparative study of paraelectric component and leakage current:

A fitting procedure was used to obtain information regarding paraelectric component and leakage current by analyzing PUND graphs. Figure 4.9 shows PUND graphs which have been fitted for further analysis. The polarization-time curve for Up cycle is linearly fitted to calculate leakage current at fixed voltage. The gradient represents magnitude of leakage current and is provided by linear fitting of curve [100]. Figure 4.10 shows that magnitude of LC and PC is lowest in sample annealed at 150°C and highest in sample annealed at 120°C. The difference in leakage current's magnitude and paraelectric componenet may be related to the variations in crystallinity among samples annealed at different temperatures.

Small crystallite size is characteristic of low crystalline specimen, however, large crystallite size is characteristic of high crystalline specimen. The increase in number of interfaces,defects and grain boundaries in substances with low crystallinity may serve as leakage current pathways. As a consequence charge carriers may become trapped at the interfaces resulting in higher leakage current [101]. The existence of defects on interfaces becomes greater as crystallite size decreases which effects paraelectric component. Defects alter lattice structure, impacting polarization alignment. They change symmetry and introduce local field therefore paraelectric effect becomes high. High-crystallinity materials often have ordered atomic structure with less defects as well as grain boundaries. The ordered structure minimizes the existence of charge carrier trapping which leads to small leakage current and paraelectric component [102].

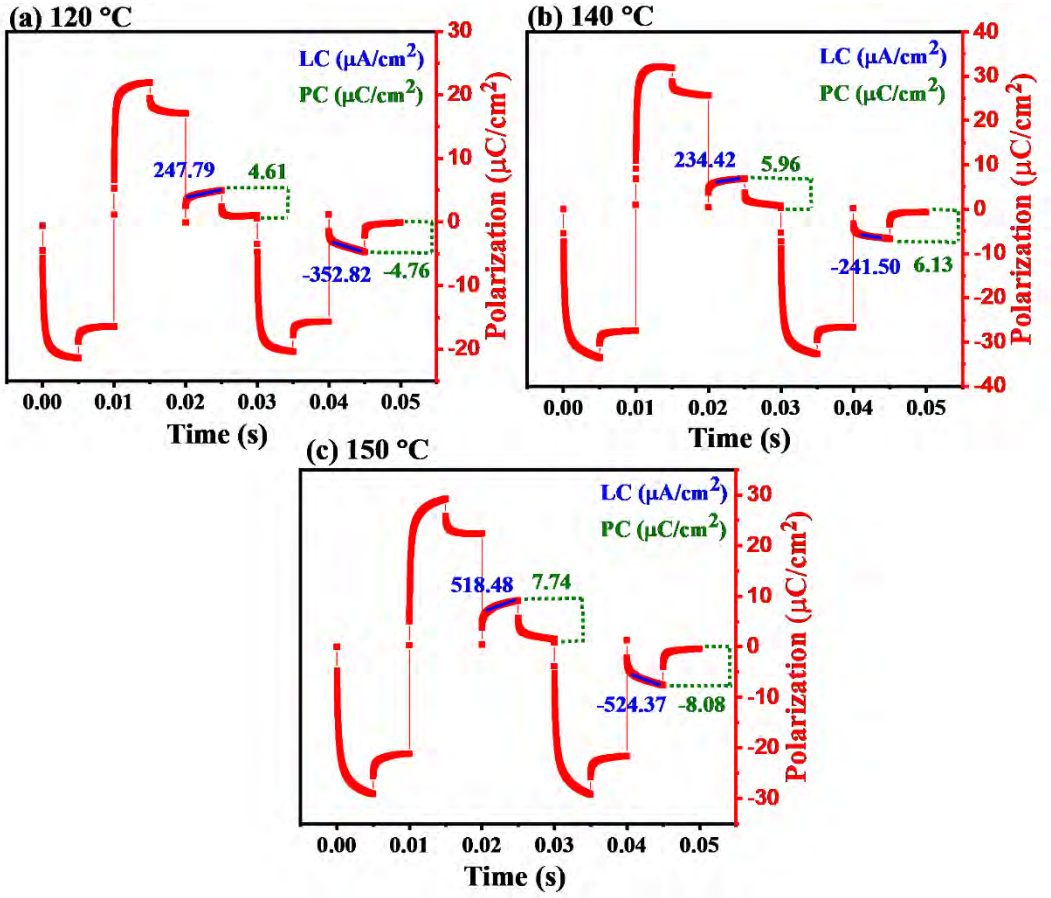

Fig: 4.9 Leakage current and Paraelectric component contributions in films annealed at (a) 120°C, (b) 140°C and (c) 150°C

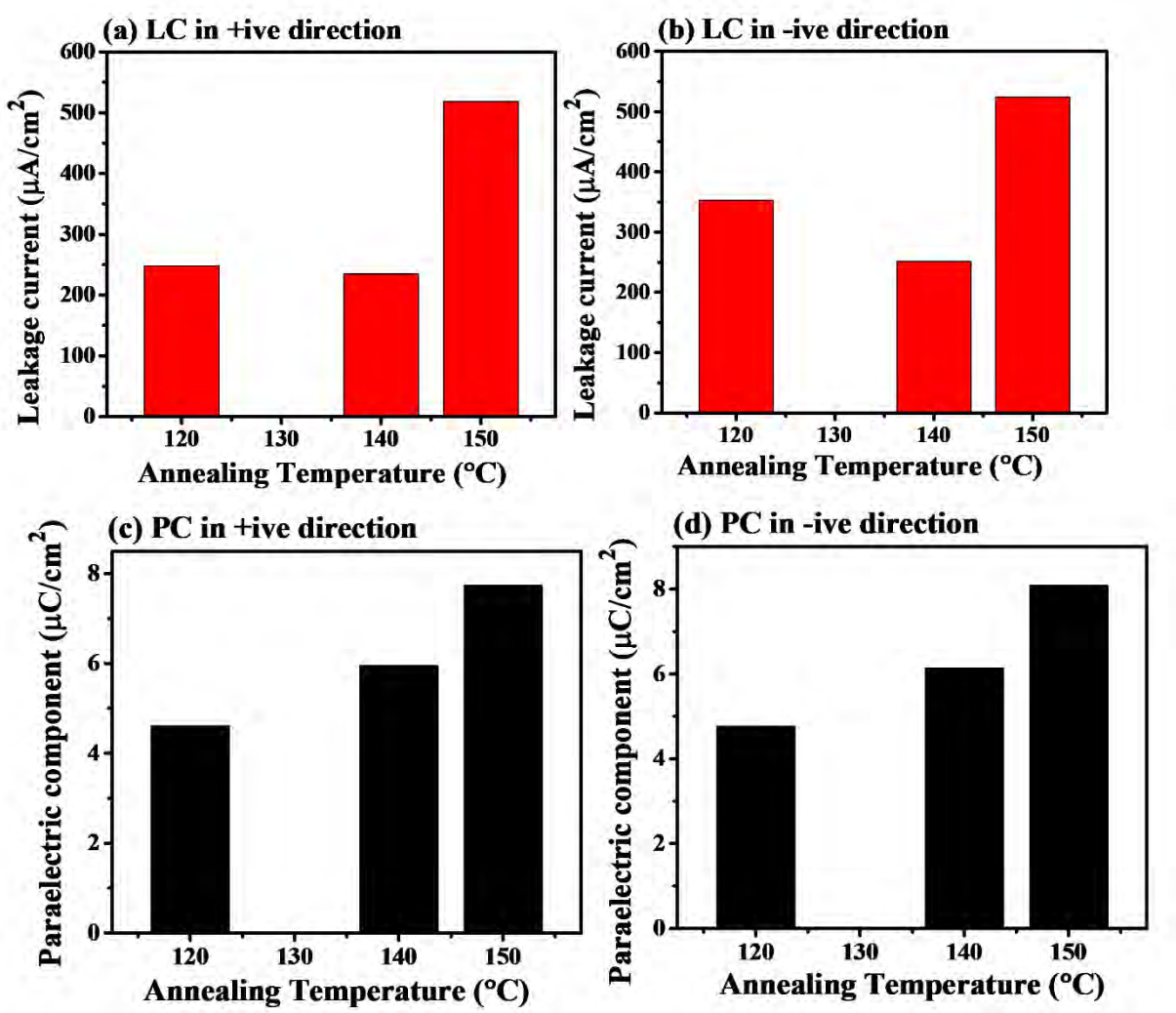

Fig: 4.10 Histogram representing Leakage current and Paraelectric component (a) LC in positive, (b) LC in negative, (c) PC in positive, (d) PC in negative directions

The magnitude of leakage current depends on the degree of crystallinity present in the samples. Film annealed at 140°C has the highest crystallinity therefore it has lowest leakage current. Whereas film annealed at 150°C has lowest crystallinity therefore it possess highest amount of leakage current.

4.1.4. Variation in remnant polarization at different applied signal frequency:

The relation between frequency and remnant polarization for PVDF TrFE thin films has been analyzed at various frequencies that range from 10Hz to 100Hz. Fig 4.11 (a) represents the loops at frequencies ranging from 10Hz to 100Hz for 2L annealed at 120°C. Fig 4.11 (b) shows loops at frequencies ranging from 10Hz to 100Hz for 2L annealed at 140°C. Fig 4.11 (c) shows loops at frequencies ranging from 10Hz to 100Hz for 2L annealed at 150°C.

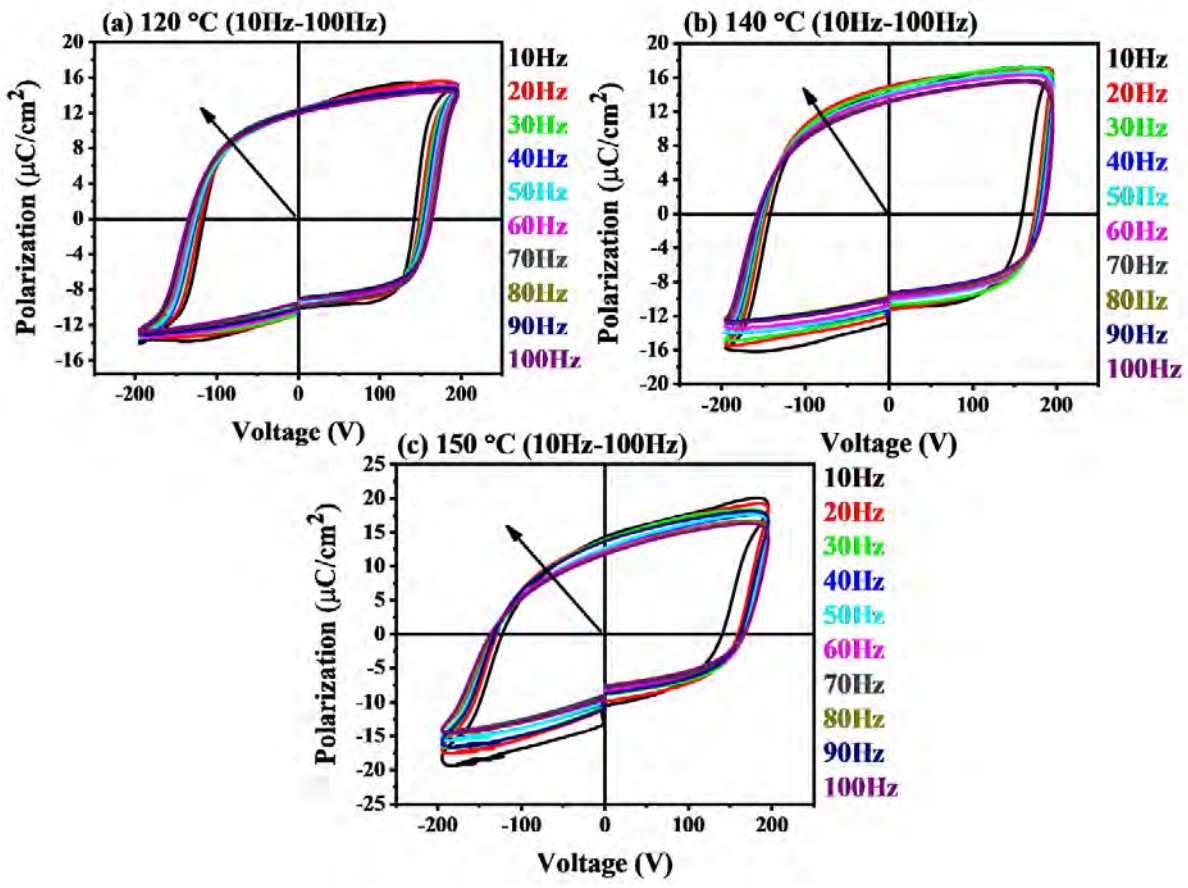

Fig: 4.11 Variation of polarization at different frequencies for thin films annealed at (a) 120°C, (b) 140°C and (c) 150°C. Arrowhead is in direction of decreasing frequency

For ferroelectric substances, shape of loop varies with frequency of electric field that is applied. At higher frequencies, the strength of the electric field is insufficient for complete saturation of domains in material, resulting in a non-symmetric loop. This implies that those domains may not be perfectly aligned with field, which results in a reduced apparent remnant polarization hence different shape of loop [103]. The loop evolves more open and nearly rectangular as the frequency of field drops. This shows that material's polarization is more readily shifted by field, resulting in an increased apparent remnant polarization and symmetrical shape of loop. The occurrence of various shapes of loop at various frequencies suggests that the strength of polarization varies with the frequency of input signal, highlighting the relevance of ferroelectric materials' frequency-dependent response [104].

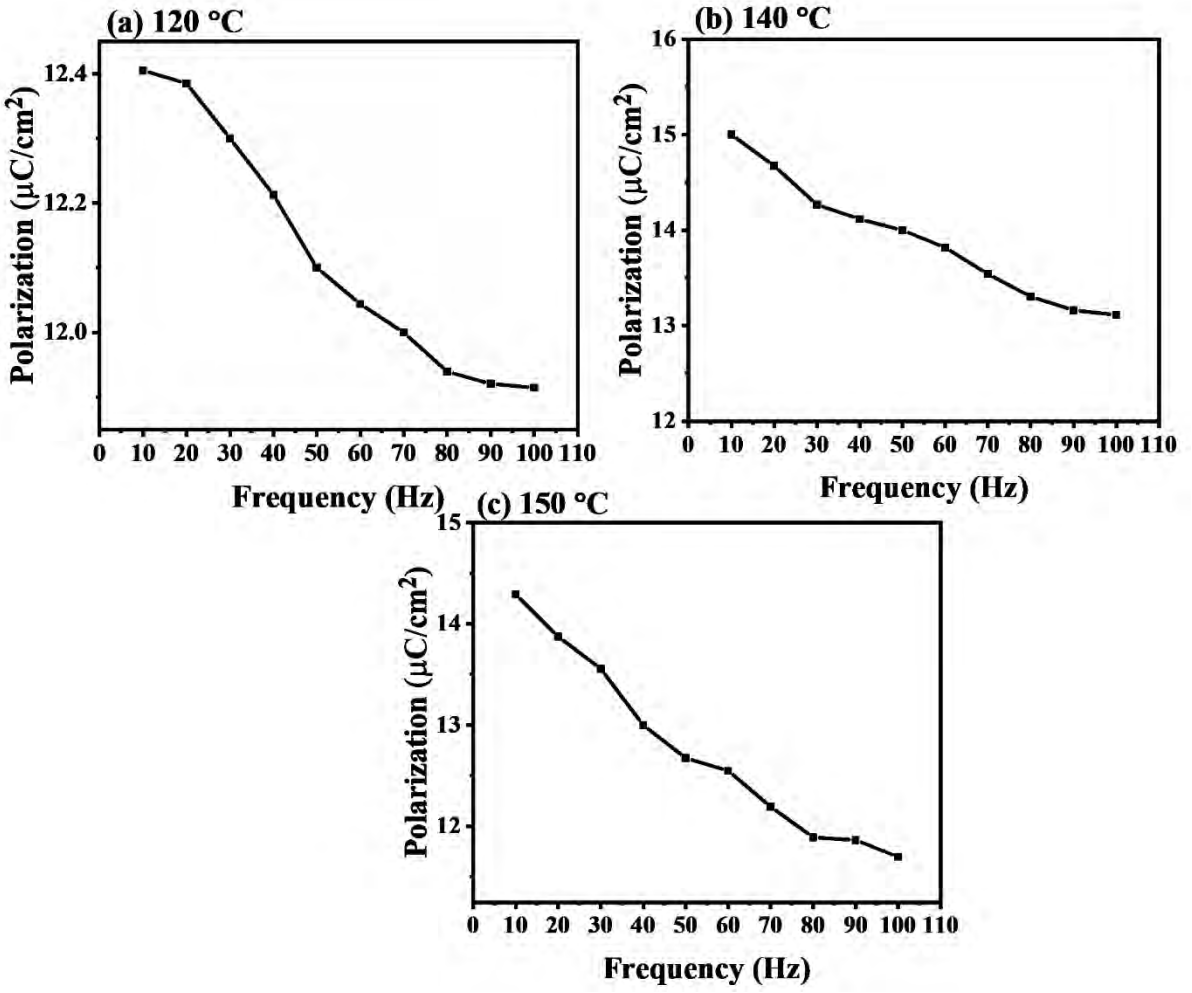

Fig: 4.12 Polarization response at different frequencies (a) 120°C, (b) 140°C and (c) 150°C

Fig 4.12 (a), (b) and (c) represent the corresponding behavior of the remnant polarization for 120°C, 140°C and 150°C respectively. If an electric field is applied to the ferroelectric substance, the dipoles prefer to align themselves along the field's direction. At high frequency, time period of applied electric field is smaller. Consequently, these dipole moments had little time for the switch, causing decrease in contribution from switching polarization to apparent remnant polarization. This occurs since a domain is unable to follow an altering electric field, limiting the mobility of dipoles. As a result, just a portion of dipoles switch, yielding a reduced switching polarization [105].

Lower frequencies, on the other hand, have a longer time interval, giving the dipoles more time for rotation and aligning them. As a result, switching polarization contributes more to the apparent remnant polarization. Furthermore, contribution of space charge polarization becomes large at frequencies that are lower. Space charge polarization involves polarization caused by the charge accumulation at the material's surfaces [106]. Both space charge and switching polarizations contributes to the apparent remnant polarization at smaller frequencies, resulting in a greater overall value. The contribution from switching polarization reduces at larger frequencies, leading to a decrease in apparent remnant polarization. Thus apparent remnant polarization diminishes as frequency gets higher [103].

4.1.5. Ferroelectric Measurement using Ag-coated sample:

In this section ferroelectric loops have been measured to investigate the behavior of polarization in P(VDF-TrFE) films using silver electrodes. Ferroelectric loops were measured at 196V and at room temperature. The sample was annealed at 130°C. Sample showed ferroelectric loop at 50Hz which confirms existence of the switching polarization. Figure 4.13 shows ferroelectric loop for P(VDF-TrFE)/Ag thin film sample.

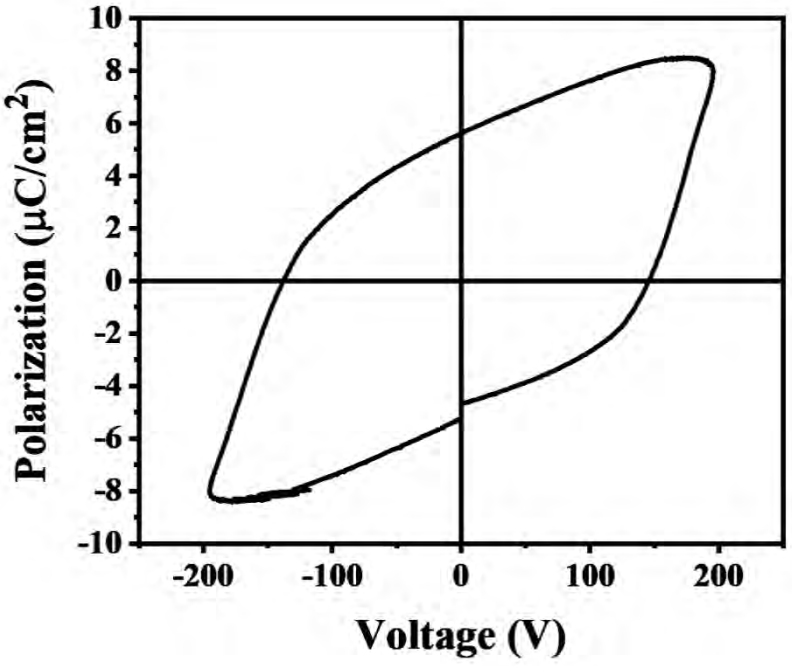

Fig: 4.13 Ferroelectric loop of P(VDF-TrFE)/Ag thin film sample

4.1.6. Comparison of Pt and Ag-coated samples:

Figure 4.14 shows ferroelectric loops of Pt and Ag-coated samples at room temperature. In present work Pt-coated samples exhibit ferroelectric loop at room temperature with frequency range of10Hz-100Hz.Whereas for Ag-coated sample we obtain loop at 50Hz. So, the data was recorded at frequency of 50Hz for comparison. In the case of Pt-coated sample we obtain a good loop but loop for Ag-coated sample looks compressed. Silver and platinum are both transition metals. When silver is exposed to the air, it tarnishes and interacts readily with chemical substances [107]. When compared with silver, platinum has a stronger corrosion resistance [108]. It's very stable and doesn't tarnish quickly. The melting point of silver is relatively low whereas platinum is the metal with the highest melting point. Platinum and silver are both good electrical conductors however silver has greater electrical conductivity over platinum [109]. Platinum is renowned for its remarkable corrosion resistance, which makes it extremely stable in a variety of electrochemical conditions. In contrast when exposed to specific substances or environment silver is more vulnerable to corrosion and tarnishing. Silver is also more prone to oxidation than platinum [110]. Therefore, in comparison with Pt metal as electrode, the low magnitude of apparent polarization obtained from Ag metal as electrode is attributed to its deteriorating characteristics and greater ability to react with environment.

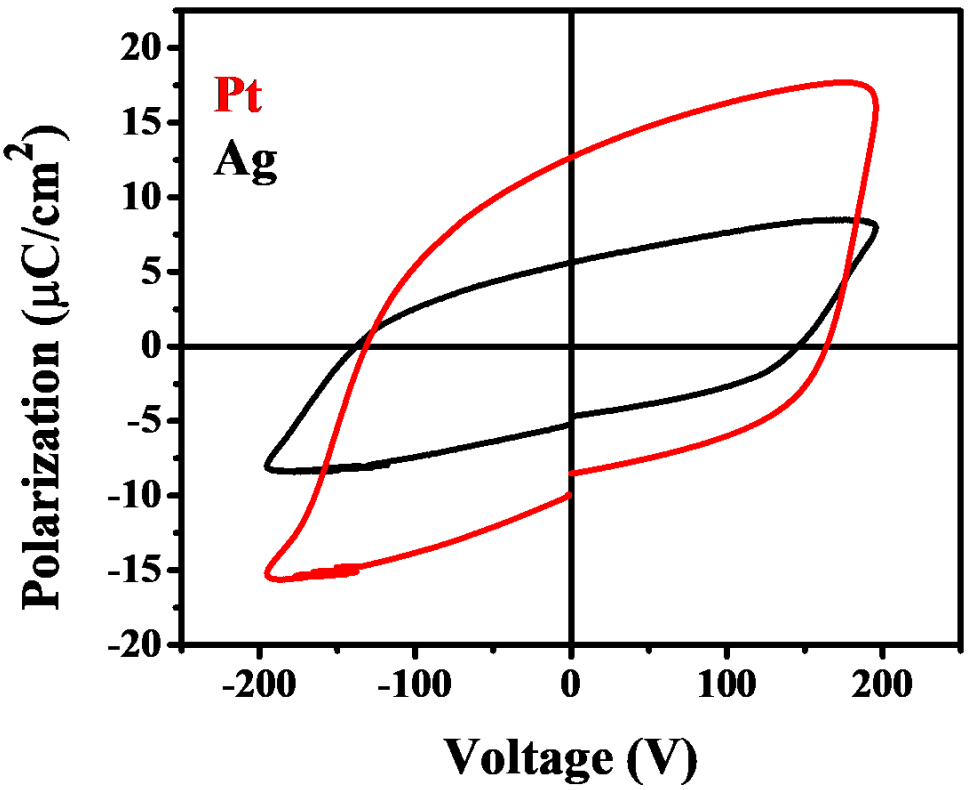

Fig: 4.14 Hysteresis loops exhibited by Pt and Ag-coated samples

The interface quality and adhesion between sample and electrode material can have a significant impact on ferroelectric behavior [111]. The bond strength between sample surface and electrode material (Ag or Pt) is commonly referred to adhesion [112]. During measurements, excellent adhesion guarantees that electrode remained properly bound to the specimen. When adhesion is fragile poor electrical connection may occur leading to inaccurate ferroelectric measurements. The charge transfer occur at interface among sample surface and electrode . An excellent interface reduces any kind of resistance which can interfere with the electrical connection or affect the ferroelectric response. The interface must be compatible with specimen [113].In our work Pt-coated specimen shows a good quality ferroelectric loop as compared to Ag-coated specimen at same voltage and frequency. The results indicate that Pt electrodes offers better adhesion as well as interface quality. It establishes an excellent bond with surface of sample enabling proper electrical contact thus minimizing interface resistance [114].

4.2. Conclusion:

The ferroelectric characteristics of P(VDF-TrFE) thin films as a function of annealing temperature were thoroughly examined in the present research. The spin coating method was used to fabricate thin films of PVDF TrFE. After spin coating films were annealed at temperature range 110°C-150°C. X-ray diffraction patterns of thin films revealed that the expected beta phase is present in each specimen. Beta phase is famous for exhibiting the desirable ferroelectric characteristics under investigation. The Annealing temperature clearly influences crystallinity of beta phase. The percentage of crystallinity for beta phase increase gradually as annealing temperature increases from 110°C to 140°C, revealing improved crystallization of films at higher annealing temperature. However, as annealing temperature rises above approaching melting temperature, the percentage of crystallinity decreases, indicating the existence of optimal annealing temperature range for crystallization of films [77]. In general, the presence of good ferroelectric loops measured at room temperature, which is consistent with XRD data, provided strong support for an effective growth of ferroelectric features in thin films. At the same voltage, apparent polarization increases with increasing annealing temperature.

PUND measurements were performed to gain an understanding of non-switching and switching behavior. The PUND measurement revealed a direct relationship between true polarization and annealing temperature because of crystallinity. The PUND results are consistent with the XRD outcomes. In each sample, apparent remnant polarization declines upon increasing the frequency. Variations in non-switching and switching polarization cause this decrease. In comparison of P(VDF-TrFE)/Pt and P(VDF-TrFE)/Ag thin films, Pt-coated specimens showed better ferroelectric loops, indicating that Pt provide greater adhesion along with interface quality. The strong bond between platinum and surface of the specimen enables optimal electrical interaction and minimizes interface resistance, leading to accurate ferroelectric measurements. On the other hand, weak adhesion and comparatively high reactivity corresponding to silver coatings might result in less reliable ferroelectric measurements.

References:

1. Eckertova, L., *Physics of thin films*. 2012: Springer Science & Business Media.
2. Messier, R.J.M.B., *Thin film deposition processes.* 1988. 13(11): p. 18-21.
3. Abegunde, O.O., et al, *Overview of thin film deposition techniques.* 2019. 6(2): p. 174-199.
4. Birnie, D.J.S.-g.t.f.g.p.a.u., *Spin coating technique.* 2004: p. 49-55.
5. Seanor, D.A., *Electrical properties of polymers*. 2013: Elsevier.
6. Dhoot, S.N., et al., *Barrier polymers.* 2002.
7. Mark, J.E., *Physical properties of polymers handbook*. Vol. 1076. 2007: Springer.
8. Park, Y.J., et al, *Control of thin ferroelectric polymer films for non-volatile memory applications.* 2010. 17(4): p. 1135-1163.
9. Zhao, C., et al., *Functional polymer thin films designed for antifouling materials and biosensors.* 2012. **66**(5): p. 323-339.
10. Zhang, Q., et al., *Critical thickness of crystallization and discontinuous change in ferroelectric behavior with thickness in ferroelectric polymer thin films.* 2001. **89**(5): p. 2613-2616.
11. Kumar, B.J.M.L., *Reply to comment on the paper "Remarkable enhancement in dielectric, piezoelectric, ferroelectric and SHG properties by iron doping in sodium para-nitrophenolatedihydrate single crystal"[Mater. Lett. 165 (2016) 99–102].* 2018. **218**: p. 360-363.
12. Jia, C., et al., *Bond electronic polarization induced by spin.* 2006. **74**(22): p. 224444.
13. Clark, A., et al., *Atomic polarization in the photodissociation of diatomic molecules.* 2006. **8**(48): p. 5591-5610.
14. Kao, K.C.J.S.P., *Dielectric phenomena in solids. 2004.* 2018: p. 94-97.
15. MDPI. *A Review: Origins of the Dielectric Properties of Proteins and Potential Development as Bio-Sensors*. 2016; Available from: https://www.mdpi.com/1424-8220/16/8/1232.
16. Khan, M.I. and T.C.J.M.F.M. Upadhyay, *General Introduction to Ferroelectrics.* 2021: p. 7.
17. Carlioz, L., et al., *Hybridization of magnetism and piezoelectricity for an energy scavenger based on temporal variation of temperature. in 2008 Symposium on Design, Test, Integration and Packaging of MEMS/MOEMS. 2008.* 2008.
18. Lang, S.B.J.P.t., *Pyroelectricity: from ancient curiosity to modern imaging tool.* 2005: p. 31.
19. Lang, S.B.J.P.t., *Pyroelectricity: from ancient curiosity to modern imaging tool.* 2005. **58**(8): p. 31.
20. Zhang, D., et al., *Recent advances in pyroelectric materials and applications.* 2021. **17**(51): p. 2103960.
21. Zhang, D., et al, *Recent advances in pyroelectric materials and applications.* 2021: p. 2103960.
22. Gate, R. *A Review on Low-Grade Thermal Energy Harvesting: Materials, Methods and Devices,Ravi Kishore,s.Jeba Priya*. Available from: https://www.researchgate.net/figure/Conceptual-model-of-pyroelectric-generator-a-Pyroelectric-materials-have-dipole_fig5_327024178.
23. Dineva, P., et al., *Piezoelectric materials*. 2014: Springer.
24. Qiu, J., H.J.I.J.o.A. Ji, and S. Sciences, *The application of piezoelectric materials in smart structures in China.* 2010: p. 266-284.
25. gate, r., *Advances in Piezoelectric Polymer Composites for Energy Harvesting Applications: A Systematic Review,Piezoelectric Effects.* 2018.
26. Xu, Y., *Ferroelectric materials and their applications*. 2013: Elsevier.
27. Martin, L.W. and A.M.J.N.R.M. Rappe, *Thin-film ferroelectric materials and their applications.* 2016. **2**(2): p. 1-14.

28. Ducharme, S., et al., *Intrinsic ferroelectric coercive field.* 2000. **84**(1): p. 175.
29. Izyumskaya, N., et al., *Processing, structure, properties, and applications of PZT thin films.* 2007. **32**(3-4): p. 111-202.
30. ResearchGate. *Characterization of domain switching and optical damage properties in ferroelectrics*. Available from: https://www.researchgate.net/figure/2-1-Ferroelectric-P-E-hysteresis-loop_fig4_266135271.
31. Benz, M. and W.B.J.J.o.a.p.s. Euler, *Determination of the crystalline phases of poly (vinylidene fluoride) under different preparation conditions using differential scanning calorimetry and infrared spectroscopy.* 2003. **89**(4): p. 1093-1100.
32. Hafner, J., et al., *Origin of the strong temperature effect on the piezoelectric response of the ferroelectric (co-) polymer P (VDF70-TrFE30).* 2019. **170**: p. 1-6.
33. Nasir, M., et al., *Control of diameter, morphology, and structure of PVDF nanofiber fabricated by electrospray deposition.* 2006. **44**(5): p. 779-786.
34. Tao, M.-m., et al., *Effect of solvent power on PVDF membrane polymorphism during phase inversion.* 2013. **316**: p. 137-145.
35. Mohammadi, B., A.A. Yousefi, and S.M.J.P.t. Bellah, *Effect of tensile strain rate and elongation on crystalline structure and piezoelectric properties of PVDF thin films.* 2007. **26**(1): p. 42-50.
36. Meng, N., et al., *Nanoscale interfacial electroactivity in PVDF/PVDF-TrFE blended films with enhanced dielectric and ferroelectric properties.* 2017. **5**(13): p. 3296-3305.
37. Sharma, M., G. Madras, and S.J.P.C.C.P. Bose, *Process induced electroactive β-polymorph in PVDF: effect on dielectric and ferroelectric properties.* 2014. **16**(28): p. 14792-14799.
38. Chen, X., X. Han, and Q.D.J.A.E.M. Shen, *PVDF-based ferroelectric polymers in modern flexible electronics.* 2017. **3**(5): p. 1600460.
39. Shepelin, N.A., et al., *New developments in composites, copolymer technologies and processing techniques for flexible fluoropolymer piezoelectric generators for efficient energy harvesting.* 2019. **12**(4): p. 1143-1176.
40. Barrau, S., et al., *Nanoscale investigations of α-and γ-crystal phases in PVDF-based nanocomposites.* 2018. **10**(15): p. 13092-13099.
41. García-Gutiérrez, M.-C., et al., *Understanding crystallization features of P (VDF-TrFE) copolymers under confinement to optimize ferroelectricity in nanostructures.* 2013. **5**(13): p. 6006-6012.
42. ResearchGate. *A Flexible Film Bulk Acoustic Resonator Based on -Phase Polyvinylidene Fluoride Polymer*. Available from: https://www.researchgate.net/figure/Structures-of-a-b-and-g-phase-polyvinylidene-fluoride-PVDF_fig1_339651923.
43. Naber, R.C., et al., *High-performance solution-processed polymer ferroelectric field-effect transistors.* 2005. **4**(3): p. 243-248.
44. Li, M., et al., *Ferroelectric phase diagram of PVDF: PMMA.* 2012. **45**(18): p. 7477-7485.
45. Bellet-Amalric, E., J.J.T.E.P.J.B.-C.M. Legrand, and C. Systems, *Crystalline structures and phase transition of the ferroelectric P (VDF-TrFE) copolymers, a neutron diffraction study.* 1998. **3**: p. 225-236.
46. Fujisaki, Y.J.F.-G.F.E.T.M.D.P. and Applications, *Poly (vinylidenefluoride-trifluoroethylene) P (VDF-TrFE)/semiconductor structure ferroelectric-gate FETs.* 2016: p. 157-183.
47. Rabe, K.M., et al., *Modern physics of ferroelectrics: Essential background*. 2007: Springer.
48. Satapathy, S., P.K. Gupta, and K.B.J.J.o.P.D.A.P. Varma, *Enhancement of nonvolatile polarization and pyroelectric sensitivity in lithium tantalate (LT)/poly (vinylidene fluoride)(PVDF) nanocomposite.* 2009. **42**(5): p. 055402.
49. Bae, I., et al., *Organic ferroelectric field-effect transistor with P (VDF-TrFE)/PMMA blend thin films for non-volatile memory applications.* 2010. **10**(1): p. e54-e57.

50. Cui, Z., et al., *Crystalline polymorphism in poly (vinylidenefluoride) membranes.* 2015. **51**: p. 94-126.
51. Fujisaki, Y.J.F.-G.F.E.T.M.D.P. and Applications, *Poly (Vinylidenefluoride-Trifluoroethylene) P (VDF-TrFE)/Semiconductor Structure Ferroelectric-Gate FETs.* 2020: p. 195-222.
52. Stephan F.Kistler and Peter M.Schweizer, *Liquid Film Coating.* 1997: p. p709-734.
53. Welchel, Z., L.A. DeSilva, and T.J.O.M. Banadara, *Properties of tris (8-hydroxyquinoline) aluminum thin films fabricated by spin coating from static and dynamic dispense methods.* 2020: p. p108.
54. Tyona, M.J.A.i.m.R., *A theoritical study on spin coating technique.* 2013: p. 195.
55. Sahu, N., B. Parija, and S.J.I.J.o.P. Panigrahi,, *Fundamental understanding and modeling of spin coating process.* 2009:p.493-502
56. Larson, R.G.a.T.J.R., *Spin coating, in Liquid Film Coating.* Springer, 1997: p. 709-734.
57. Lawrence, C.J.T.P.o.f., *The mechanics of spin coating of polymer films.* 1988: p. 2786-2795.
58. Sadegh-cheri, M., Design, *Design, fabrication, and optical characterization of a low-cost and open-source spin coater.* ACS Publications, 2019.
59. DEVTECH&CP, V.-f.S.-c.U.i.g., Vacuum-free Spin-coater Unit in glovebox. and E441 (Ossila Ltd). *E441 (Ossila Ltd),*. 2021; s]. Available from: http://www.devtechcp.eu/facilities/.
60. Mao, D., et al., *Optimization of poly (vinylidene fluoride-trifluoroethylene) films as non-volatile memory for flexible electronics.* 2010. **11**(5): p. 925-932.
61. Jung, S.-W., et al., *Properties of ferroelectric P (VDF-TrFE) 70/30 copolymer films as a gate dielectric.* 2008. **100**(1): p. 198-205.
62. B.V, L.B. *LabMakelaar Banelux B.V,Branson Sonifier 250 Cell Disruptor*. 2022 [17-03-2023]; Available from: https://www.labmakelaar.eu/shop/all/saleable/dissolution-stirring-and-shaking/other-stirring-and-shaking/branson-sonifier-250-cell-disruptor/.
63. Smentkowski, V.S.J.P.i.S.S., *Trends in sputtering.* 2000: p. 1-58.
64. Thornton, J.A.J.S.T., *Sputter Coating—Its Principles and Potential.* 1973:p.1787-1805.
65. FISIKA, P.P. *Mini Plasma Sputtering Coater*. Available from: http://www.fisika.lipi.go.id/fasilitas/detil/mini-plasma-sputtering-coater.
66. Thornton, J.A.J.S.T., *Sputter Coating—Its Principles and Potential.* 1973: p. 1787-1805.
67. B.D.CUILITY, *Elements of X-ray Diffraction, Second edition.* 1978: p. 88-91.
68. Epp, J., *X-ray diffraction (XRD) techniques for materials characterization*, in *Materials characterization using nondestructive evaluation (NDE) methods*. 2016, Elsevier. p. 81-124.
69. Chegg , W.S., Javad Hashemi, William F Smith, *Foundations of Materials Science and Engineering.* McGraw-Hill Science/Engineering/Math (4/9/2009): p. 22.
70. B.D.CUILITY, *Elements of X-ray Diffraction, Second edition.* 1978: p. 86-88.
71. Web, A.C.i.P.D.o.t. and C. Index. *Bragg's Law*. Available from: http://pd.chem.ucl.ac.uk/pdnn/powintro/braggs.htm.
72. TECHNOLOGIES.INC., R. *Test Station for Thin Films*. Available from: https://www.ferrodevices.com/tester-accessories/test-stations-for-thin-films/.
73. Kow, K.-C., *Dielectric Phenomenon in Solids 1st edition.* 2004:p.217.
74. ResearchGate. *Schematic representation of Sawyer-Tower hysteresis loop measurement technique*. Available from: https://www.researchgate.net/figure/Schematic-representation-of-Sawyer-Tower-hysteresis-loop-measurement-technique-Adapted_fig4_259759119.
75. Hafner, J., et al.,, *Large bias-induced piezoelectric response in the ferroelectric polymer P (VDF-TrFE) for MEMS resonators.* 2021: p. 195-203.

76. PSI, P.S.I. *Thin Films,Spin Coating*. Available from: https://www.psi.ch/en/lmx-interfaces/thin-films-methods.
77. Feng, T., et al., *Temperature control of P (VDF-TrFE) copolymer thin films.* 2013. **141**(1): p. 187-194.
78. Shigesato, Y., et al., *Early stages of ITO deposition on glass or polymer substrates.* 2000. **59**(2-3): p. 614-621.
79. Li, W., et al., *Annealing effect on poly (vinylidene fluoride/trifluoroethylene)(70/30) copolymer thin films above the melting point.* 2010. **116**(2): p. 663-667.
80. Kimura, K., et al., *Orientation control of ferroelectric polymer molecules using contact-mode AFM.* 2004. **40**(5): p. 933-938.
81. Gao, X., et al., *Application of Three-Vapor Recompression Heat-Pump Concepts to a Dimethylformamide–Water Distillation Column for Energy Savings.* 2014. **2**(3): p. 250-256.
82. Schenk, T., et al., *About the deformation of ferroelectric hystereses.* 2014. **1**(4).
83. Wong, C., C. Tsang, and F.J.J.o.a.p. Shin, *Explicit expressions for the dynamic polarization behavior in ferroelectrics with symmetric/asymmetric electrical conductivity.* 2004. **96**(1): p. 575-583.
84. Prume, K., et al., *Dynamic leakage current compensation in ferroelectric thin-film capacitor structures/Meyer, René; Waser, Rainer; Prume, Klaus; Schmitz, Torsten; Tiedke, Stephan.*
85. Meyer, R., et al., *Dynamic leakage current compensation in ferroelectric thin-film capacitor structures.* 2005. **86**(14): p. 142907.
86. Song, Z., et al., *Effect of Current Density on the Performance of Ni–P–ZrO2–CeO2 Composite Coatings Prepared by Jet-Electrodeposition.* 2020. **10**(7): p. 616.
87. Seo, J., J.Y. Son, and W.-H.J.M.L. Kim, *Structural and ferroelectric properties of P (VDF-TrFE) thin films depending on the annealing temperature.* 2019. **238**: p. 294-297.
88. Khan, M., U.S. Bhansali, and H.N.J.O.E. Alshareef, *Fabrication and characterization of all-polymer, transparent ferroelectric capacitors on flexible substrates.* 2011. **12**(12): p. 2225-2229.
89. Park, Y.J., et al., *Recovery of remanent polarization of poly (vinylidene fluoride-co-trifluoroethylene) thin film after high temperature annealing using topographically nanostructured aluminium bottom electrode.* 2007. **90**(22): p. 222903.
90. Li, W., et al., *Crystalline morphologies of P (VDF-TrFE)(70/30) copolymer films above melting point.* 2008. **254**(22): p. 7321-7325.
91. Park, Y.J., et al., *Irreversible extinction of ferroelectric polarization in P (VDF-TrFE) thin films upon melting and recrystallization.* 2006. **88**(24): p. 242908.
92. Ohigashi, H., S. Akama, and K.J.J.j.o.a.p. Koga, *Lamellar and bulk single crystals grown in annealed films of vinylidene fluoride and trifluoroethylene copolymers.* 1988. **27**(11R): p. 2144.
93. Naganuma, H., Y. Inoue, and S.J.J.j.o.a.p. Okamura, *Estimation of leakage current density and remanent polarization of BiFeO3 films with low resistivity by positive, up, negative, and down measurements.* 2008. **47**(7R): p. 5558.
94. Hu, W., et al., *Space-Charge-Mediated Anomalous Ferroelectric Switching in P (VDF–TrEE) Polymer Films.* 2014. **6**(21): p. 19057-19063.
95. Bhansali, U.S., M. Khan, and H.N.J.M.e. Alshareef, *Organic ferroelectric memory devices with inkjet-printed polymer electrodes on flexible substrates.* 2013. **105**: p. 68-73.
96. Samanta, S., V. Sankaranarayanan, and K.J.J.o.M.S.M.i.E. Sethupathi, *Effect of Nb and Fe co-doping on microstructure, dielectric response, ferroelectricity and energy storage density of PLZT.* 2018. **29**(23): p. 20383-20394.
97. Xia, F., et al., *Dependence of threshold thickness of crystallization and film morphology on film processing conditions in poly (vinylidene fluoride–trifluoroethylene) copolymer thin films.* 2002. **92**(6): p. 3111-3115.

98. Prabu, A.A., K.J. Kim, and C.J.V.S. Park, *Effect of thickness on the crystallinity and Curie transition behavior in P (VDF/TrFE)(72/28) copolymer thin films using FTIR-transmission spectroscopy.* 2009. **49**(2): p. 101-109.
99. Xiao, Y., et al., *Ferroelectric Properties and Leakage Behavior in Poly (Vinylidene Fluoride-Trifluoroethylene) Ferroelectric Thin Films with Additive Diethyl Phthalate.* 2011. **125**(1): p. 89-97.
100. Zongyuan, F., et al., *Improved Thermal Stability of Ferroelectric Phase in Epitaxially Grown P (VDF-TrFE) Thin Films.* 2016.
101. Fu, Z., et al., *Improved thermal stability of ferroelectric phase in epitaxially grown P (VDF-TrFE) thin films.* 2016. **49**(10): p. 3818-3825.
102. Naganuma, H., Y. Inoue, and S.J.A.p.e. Okamura, *Evaluation of electrical properties of leaky BiFeO3 films in high electric field region by high-speed positive-up–negative-down measurement.* 2008. **1**(6): p. 061601.
103. Chaipanich, A., N. Jaitanong, and R.J.F.L. Yimnirun, *Ferroelectric hysteresis behavior in 0-3 PZT-cement composites: effects of frequency and electric field.* 2009. **36**(3-4): p. 59-66.
104. Krohns, S. and P.J.P.S.R. Lunkenheimer, *Ferroelectric polarization in multiferroics.* 2019. **4**(9).
105. Mai, M., A. Leschhorn, and H.J.P.B.C.M. Kliem, *The field and temperature dependence of hysteresis loops in P (VDF–TrFE) copolymer films.* 2015. **456**: p. 306-311.
106. Rayssi, C., et al., *Frequency and temperature-dependence of dielectric permittivity and electric modulus studies of the solid solution Ca 0.85 Er 0.1 Ti 1− x Co 4x/3 O 3 (0≤ x≤ 0.1).* 2018. **8**(31): p. 17139-17150.
107. Cataldi, T.R., et al., *Comparison of silver, gold and modified platinum electrodes for the electrochemical detection of iodide in urine samples following ion chromatography.* 2005. **827**(2): p. 224-231.
108. Al-Shara, N.K., et al., *Electrochemical investigation of novel reference electrode Ni/Ni (OH)* ₂ *in comparison with silver and platinum inert quasi-reference electrodes for electrolysis in eutectic molten hydroxide.* 2019. **44**(50): p. 27224-27236.
109. Isebeck, K. and K.J.R.E. Poole, *Comparison of stage i of the recovery of thermal and fast neutron damage in copper, silver and platinum.* 1974. **22**(1): p. 15-27.
110. Chatenet, M., et al., *Oxygen reduction on silver catalysts in solutions containing various concentrations of sodium hydroxide–comparison with platinum.* 2002. **32**(10): p. 1131-1140.
111. Pintilie, I., et al., *The impact of the Pb (Zr, Ti) O3-ZnO interface quality on the hysteretic properties of a metal-ferroelectric-semiconductor structure.* 2012. **112**(10): p. 104103.
112. Pulker, H., A. Perry, and R.J.S.T. Berger, *Adhesion.* 1981. **14**(1): p. 25-39.
113. Lin, Y. and C.J.J.o.m.s. Chen, *Interface effects on highly epitaxial ferroelectric thin films.* 2009. **44**: p. 5274-5287.
114. Lee, Y., et al., *The influence of top and bottom metal electrodes on ferroelectricity of hafnia.* 2021. **68**(2): p. 523-528.